NASA CR-179464
GTD86-5

INVESTIGATION OF A REPETITIVE PULSED ELECTROTHERMAL THRUSTER

by R. L. Burton, D. Fleischer, S. A. Goldstein,
D. A. Tidman and N. K. Winsor

GT-Devices, Inc.

August 21, 1986

prepared for

NATIONAL AERONAUTICS AND SPACE ADMINISTRATION

NASA-Lewis Research Center
Contract NAS3-24636

1. Report No.	2. Government Accession No.	3. Recipient's Catalog No.
CR-179464		

4. Title and Subtitle	5. Report Date
Investigation of a Repetitive Pulsed Electrothermal Thruster	August 21, 1986
	6. Performing Organization Code

7. Author(s)	8. Performing Organization Report No.
R. L. Burton, D. Fleischer, S. A. Goldstein and D. A. Tidman	GTD Rpt. No. 86-5
	10. Work Unit No.

9. Performing Organization Name and Address	11. Contract or Grant No.
GT-Devices, Inc. 5705A General Washington Drive Alexandria, VA 22312	NAS3-24636
	13. Type of Report and Period Covered Contract Report 5/24/85 - 5/23/86

12. Sponsoring Agency Name and Address	14. Sponsoring Agency Code
National Aeronautics and Space Administration Washington, DC 20546	

15. Supplementary Notes

Project Manager, Lynnette M. Zana
NASA-Lewis Research Center
Cleveland, Ohio

16. Abstract

A pulsed electrothermal (PET) thruster with 1000:1 ratio nozzle is tested in a repetitive mode on water propellant. The thruster is driven by a 60J pulse forming network at repetition rates up to 10 Hz (600W). The pulse forming network has a .31 ohm impedance, well matched to the capillary discharge resistance of .40 ohm, and is directly coupled to the thruster electrodes without a switch. The discharge is initiated by high voltage breakdown, typically at 2500V, through the water vapor in the interelectrode gap. Water is injected as a jet through a .37 mm orifice on the thruster axis. Thruster voltage, current and impulse bit are recorded for several seconds at various power supply currents. Thruster to power ratio is typically T/P = .07 N/kW. Tank background pressure precludes direct measurement of exhaust velocity which is inferred from calculated pressure and temperature in the discharge to be about 14 km/sec. Efficiency, based on this velocity and measured T/P is .54 ± .07. Thruster ablation is zero at the throat and becomes measurable further upstream, indicating that radiative ablation is occurring late in the pulse.

17. Key Words (Suggested by Author(s))	18. Distribution Statement
Electric Propulsion Electrothermal Thruster Liquid Propellant	Unclassified - Unlimited

19. Security Classif. (of this report)	20. Security Classif. (of this page)	21. No. of pages	22. Price*
Unclassified	Unclassified	59	

*For sale by the National Technical Information Service, Springfield, Virginia 22161

TABLE OF CONTENTS

SUMMARY

Pulsed Electrothermal (PET) propulsion is a technique for avoiding the material temperature limitations of steady electrothermal propulsion, by operating an electrothermal thruster at megawatt power levels for microsecond time scales. By varying the energy per pulse and the pulse rate, operating parameters can in principle always be found which prevent the electrodes and insulator from reaching the melting point. A second benefit of pulsed operation comes from the several hundred atmosphere pressure levels achieved during the pulse. The supersonic nozzle flow is then in equilibrium rather than in a frozen state, so that the ionization energy of the propellant is recovered in the nozzle. In addition, the high Reynolds number in the nozzle allows the nozzle flow to be treated as inviscid.

The work presented in this report establishes technical feasibility for a repetitive PET thruster using a liquid water propellant. The use of water allows the thruster to operate in a non-ablative mode, and permits the use of conventional liquid propellant tanks, valves and filters. In addition, the thruster is operated without a switch, thus eliminating this possibly troublesome component from the system.

The thruster is driven by a .31 ohm, 16 microfarad, 60J, capacitive pulse forming network which is directly coupled to the electrodes. The thruster resistance is 0.4 ohm, so that the

capacitors do not "ring", an important factor for capacitor life. The mean discharge power is several megawatts, which when integrated over the pulse gives a discharge energy which is 99% of the stored energy. This high transfer efficiency is a result of the 0.4 ohm thruster resistance and transmission and capacitor internal losses of less than .004 ohms.

The thruster is mounted on a calibrated thrust stand, and the thrust impulse bit is measured from the thrust stand recoil after each shot. The ratio of impulse bit to stored energy, $\int Tdt/E$, is equivalent to thrust to power ratio, N/kW. The measured values in these experiments are .06 - .08 N/kW.

High tank background pressures preclude direct exhaust velocity measurements. Instead, exhaust velocity is estimated from theory and from comparison with previous experiments. Exhaust velocity is calculated as 14 km/sec for water at 20,000°K, expanded in the nozzle. This velocity is consistent with previously measured velocities of 27 km/sec for a PET thruster with a solid polyethylene propellant liner [1-2]. It is calculated that operation in a hard vacuum would raise the exhaust velocity from 14 to 17 km/sec with a 1000:1 area ratio nozzle.

In previous experiments, the efficiency of an ablating wall PET thruster was found to be .37-.42 for polyethylene propellant at 1500-1750 sec. In this experiment, the efficiency, found from the measured thrust and calculated exhaust velocity, is $\eta = .54 \pm .08$.

It is predicted that operation in a better vacuum would raise the efficiency to the .65-.80 range.

The work reported here demonstrates the technical feasibility of the PET thruster, which when coupled with its superior performance in the 1000-2000 second specific impulse range, justifies serious consideration of PET for a number of space propulsion missions.

I. INTRODUCTION

The pulsed electrothermal (PET) thruster, essentially a high resistance, high pressure electrothermal discharge coupled to a supersonic nozzle, has been proposed as a way to achieve high efficiency in the 1000-2000 second specific impulse range. This I_{sp} range is of particular interest for a number of near-earth missions ranging from attitude control to primary propulsion. This is because propellant savings are significant in comparison to chemical thrusters, yet the thrust is high enough that thrust times are not excessive.

The major goal of PET thruster development is to provide sufficient system lifetime and efficiency (over .50) to justify the modest increase in system complexity from DC systems. A comparison of predicted PET-thruster performance for water and liquid hydrogen propellant is compared to that for competing electric thrusters in Figure 1. It can be seen that no existing system except PET is a candidate for high efficiency at 1000-2000 seconds.

In a previous report [1], data was presented on a PET thruster for which the discharge pressure was contained by a solid polyethylene liner which ablated to feed polyethylene propellant to the arc. The next report [2] refined the performance measurements for the ablating polyethylene thruster, and presented a conceptual design for a PET thruster system fed by easily stored liquid water. Subsequently, preliminary experiments were conducted at GT-Devices

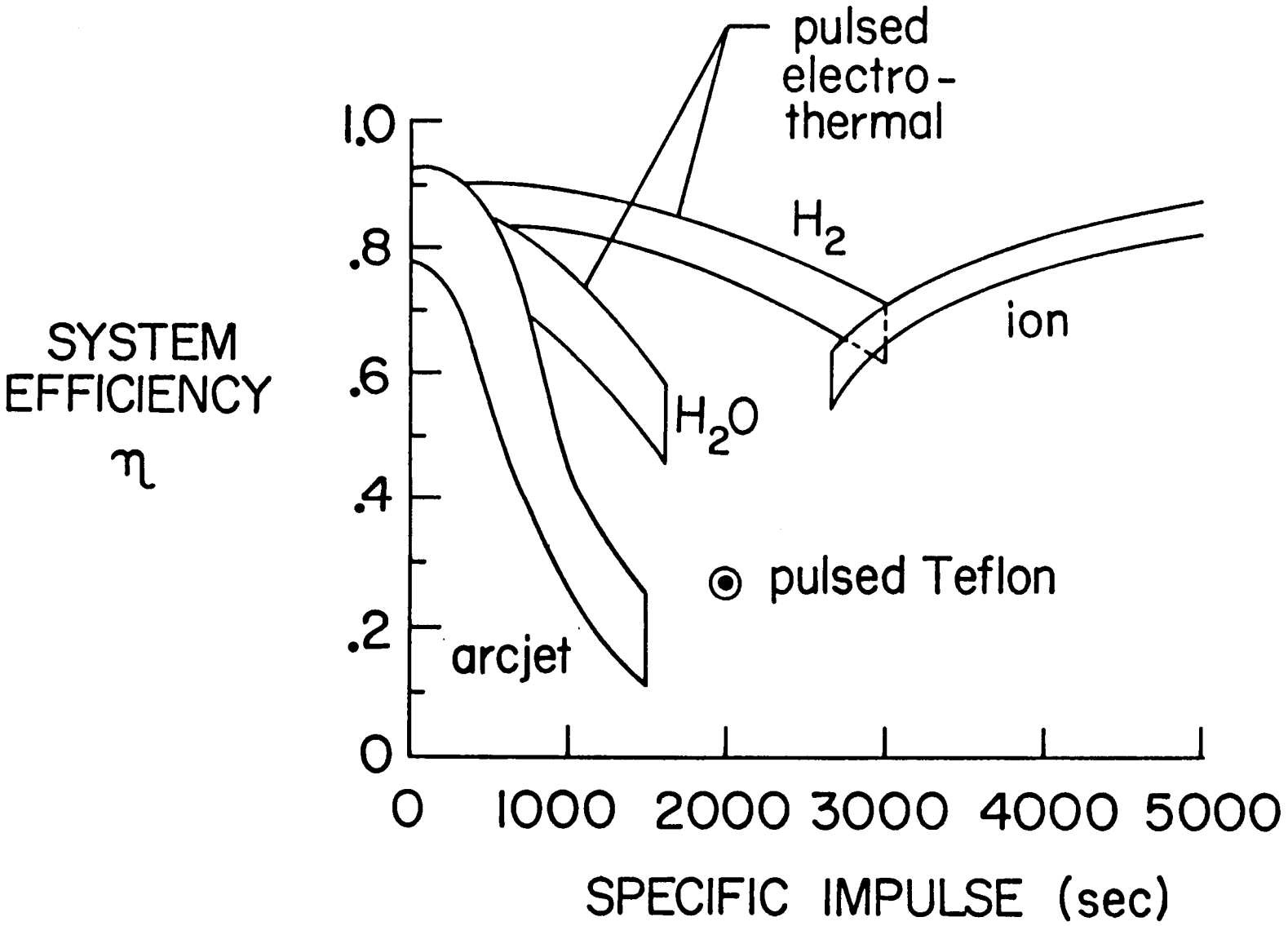

Figure 1. COMPARISON OF PET WITH COMPETING ELECTRIC THRUSTERS

to verify PET thruster operation with water propellant, and to measure the breakdown field strength for the device [3].

In the previous experiments, the efficiency of the ablating wall PET thruster was found to be .37-.42 for polyethylene propellant at 1500-1750 seconds specific impulse. It was felt that this efficiency could be improved by a number of design changes.

In the present experiments, the PET thruster is designed to operate in a repetitive mode without a switch or a pulsed propellant valve. The thruster capacitors are allowed to charge to the breakdown voltage, and then directly discharge to the thruster electrodes. This operational mode simplifies the thruster system at the expense of small shot-to-shot variations in thruster impulse. Thermal losses are reduced by moving the nozzle electrode into the throat, by increasing the nozzle area ratio to 1000:1, and by operating at a lower arc temperature.

The present work is a technical feasibility study, then, for a new type of electrothermal thruster. The goal is to operate at a mean power of several hundred watts using water propellant in a pulsed mode, and to achieve significantly higher efficiencies than other electric thrusters in the 1000-2000 second range. The successful results of this effort are presented below.

II. REPETITIVE PET THRUSTER OPERATION

The water-injected PET thruster used in this experiment (Fig. 2) operates at a megawatt power level by discharging small amounts of energy (40-80J) on a microsecond time scale. The water subjected to this power level has a mass of only a few milligrams, and is heated to 15,000-25,000 °K, at a pressure of 200-1000 atmospheres (3000-15,000 psi). Because of the high discharge pressure, flow in the nozzle is in equilibrium, and in a high area ratio nozzle the ionization energy is completely recovered. The exhaust flow therefore consists entirely of water molecules and products of dissociation.

In order to withstand the high heat transfer rates in the thruster, the power is supplied to the electrodes in a short pulse. The standard technique for supplying low energy, short duration pulses is the capacitive pulse forming network (PFN). The capacitors used in this investigation are off-the-shelf units from Aerovox (SX32H, 2 microfarad, 8 KVDC) which are designed for repetitive operation. The main drawback in the use of these capacitors is their high internal inductance of 0.5 microhenries. This is overcome by paralleling the capacitors, so that the initial PFN design used a 2-2-2 arrangement of capacitors, connected with 0.4 microhenry inductors. The Princeton Circuit Analysis Program (PCAP)[4] code prediction for this arrangement indicated that the tail of the pulse would droop excessively, so that a 2-2-4 arrangement was tried, and proved successful. The PFN and the

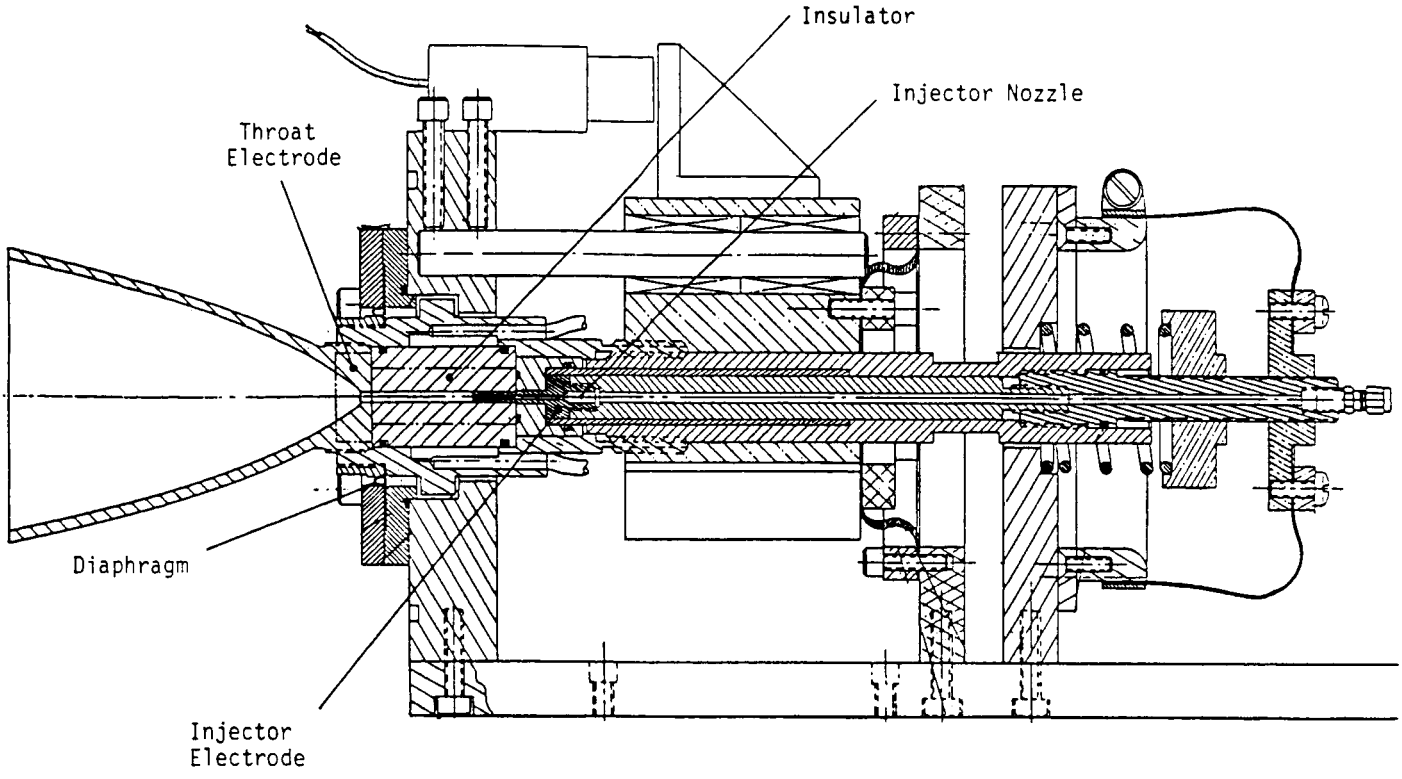

Figure 2a. PET THRUSTER AND THRUST STAND ASSEMBLY

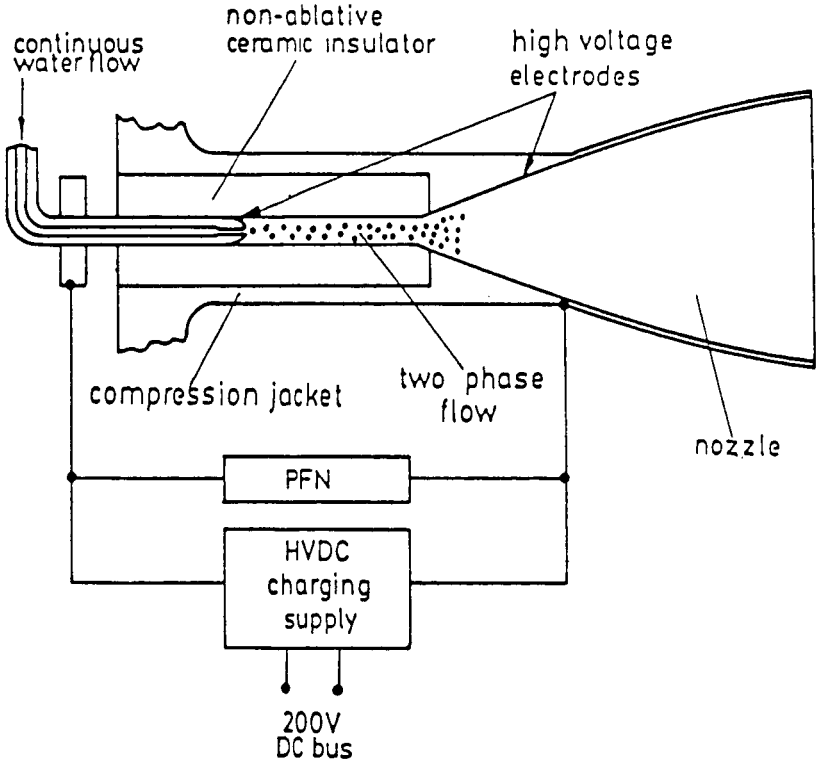

Figure 2b. WATER PROPELLANT PET THRUSTER SCHEMATIC

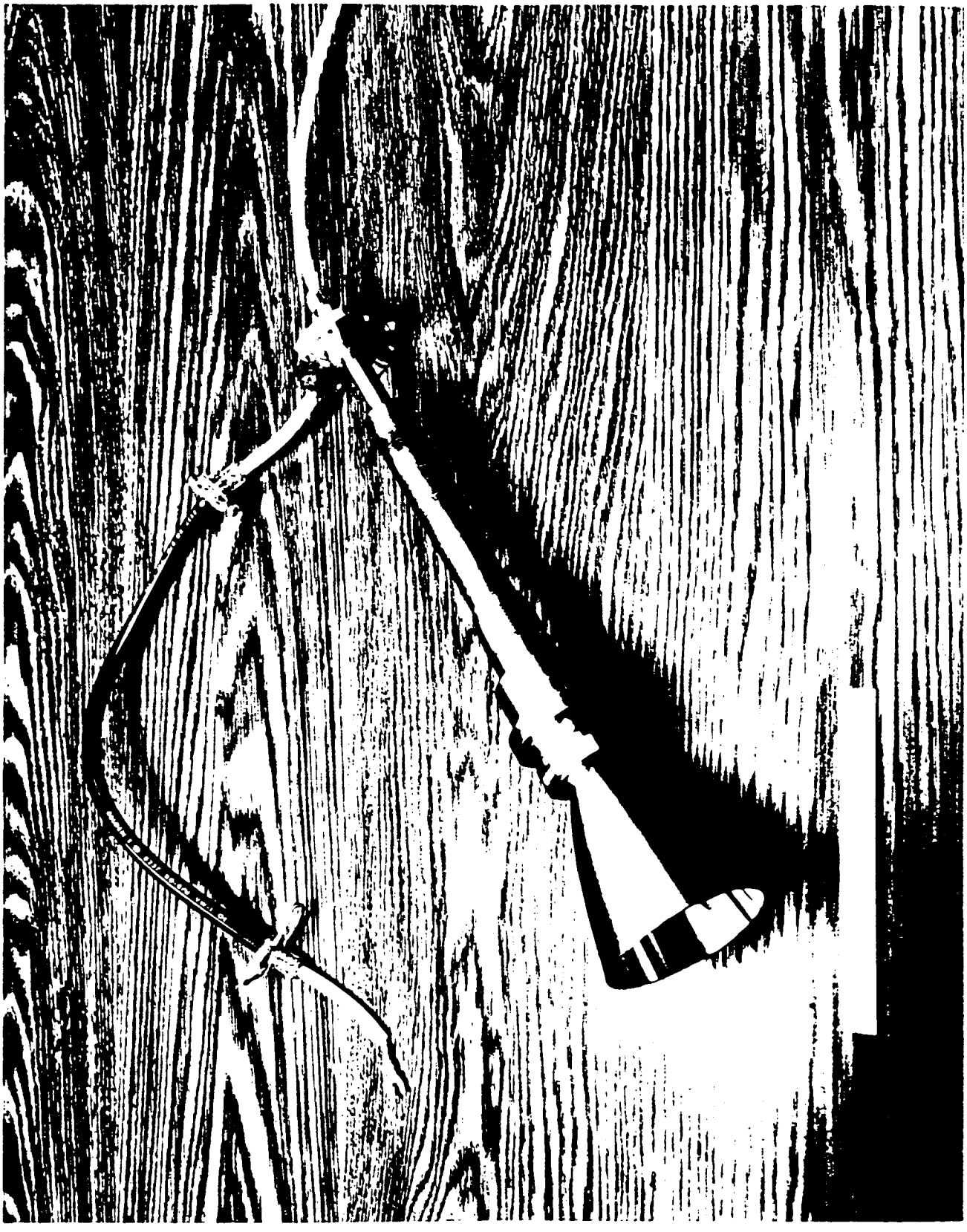

Figure 2b. WATER PROPELLANT PET THRUSTER

resulting current pulse are shown in Figure 3. The FWHM of the pulse is 12 microseconds, and peak current is several kA.

As shown in Figure 3, the PFN is directly coupled to the PET thruster. This mode of operation was previously demonstrated by GT-Devices, using water propellant.[3]. The power supply is regulated for constant current, so that the capacitor voltage rises linearly with time until a breakdown voltage is reached and the pulse begins. The total energy discharged depends on the breakdown voltage, and thus varies somewhat from shot to shot as shown in Figure 4. The variation is small enough, however, so that the thrust is constant when averaged over a few tens of pulses. This is shown in the thrust stand response curves of Fig. 4.

The experiments were conducted in a GT-Devices vacuum tank (Figs. 5 and 6) with a volume of 1 m^3. With a roughing pump (Welch #1397), the tank can be pumped down to less than 1 torr. With propellant flowing the pump cannot keep up, and the pressure is 10-20 torr, as determined by the vapor pressure of the water. Unfortunately, this rather high pressure precludes measurement of the exhaust velocity by time-of-flight techniques, as will be discussed in the next section.

Diagnostics for PET thruster performance measurements are the same as those reported previously [1-2]. The current is measured by a passively integrated Rogowski coil. Voltage is measured by a 1000:1 Tektronics probe. PFN capacitance is checked on a bridge,

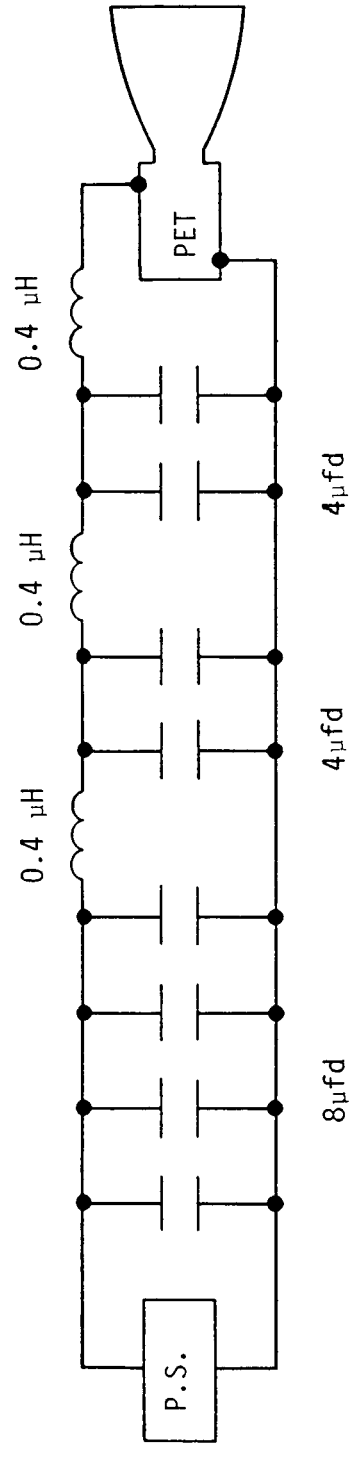

Figure 3a. PET THRUSTER ELECTRICAL SCHEMATIC

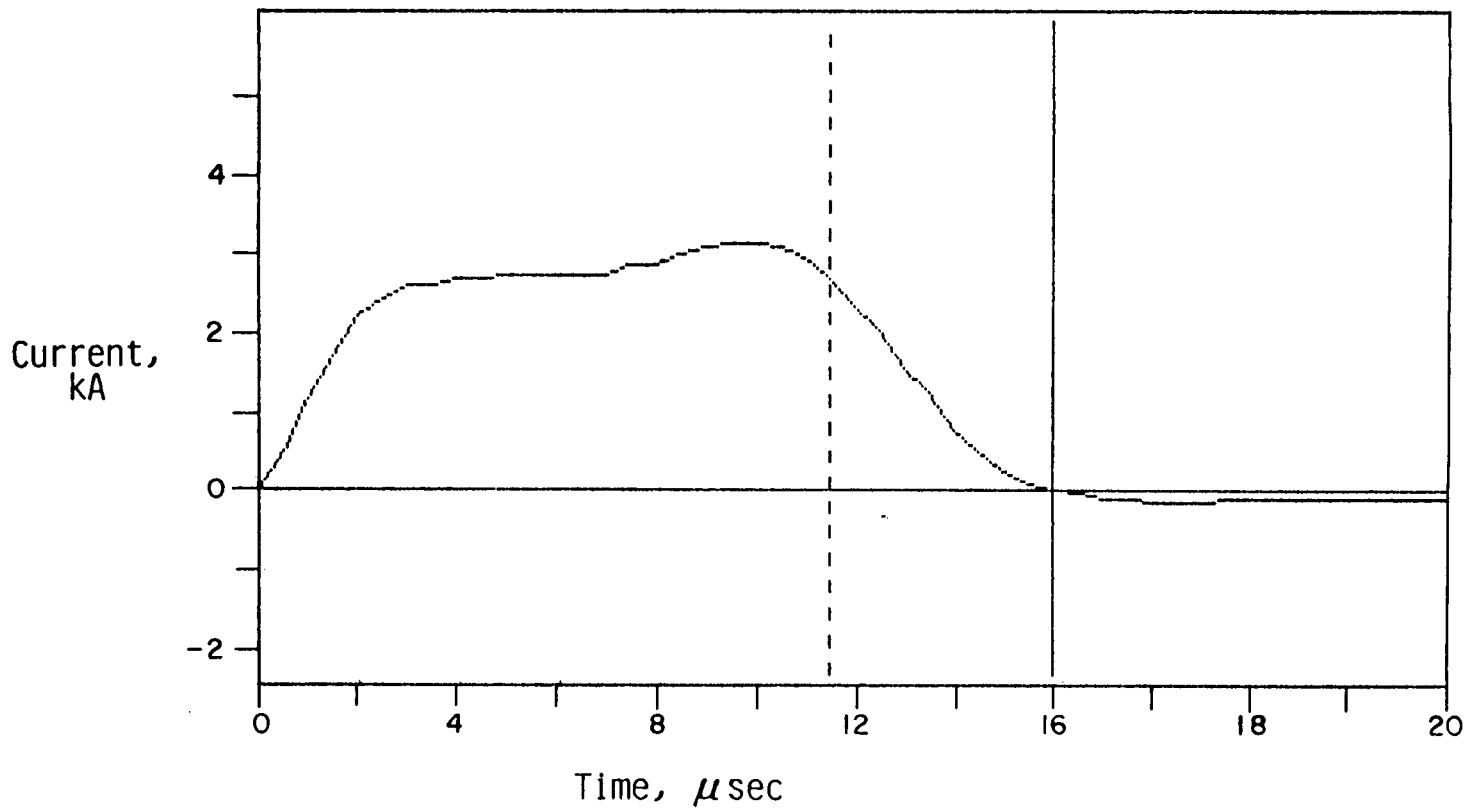

Figure 3b. CURRENT PULSE TO PET THRUSTER FROM PFN

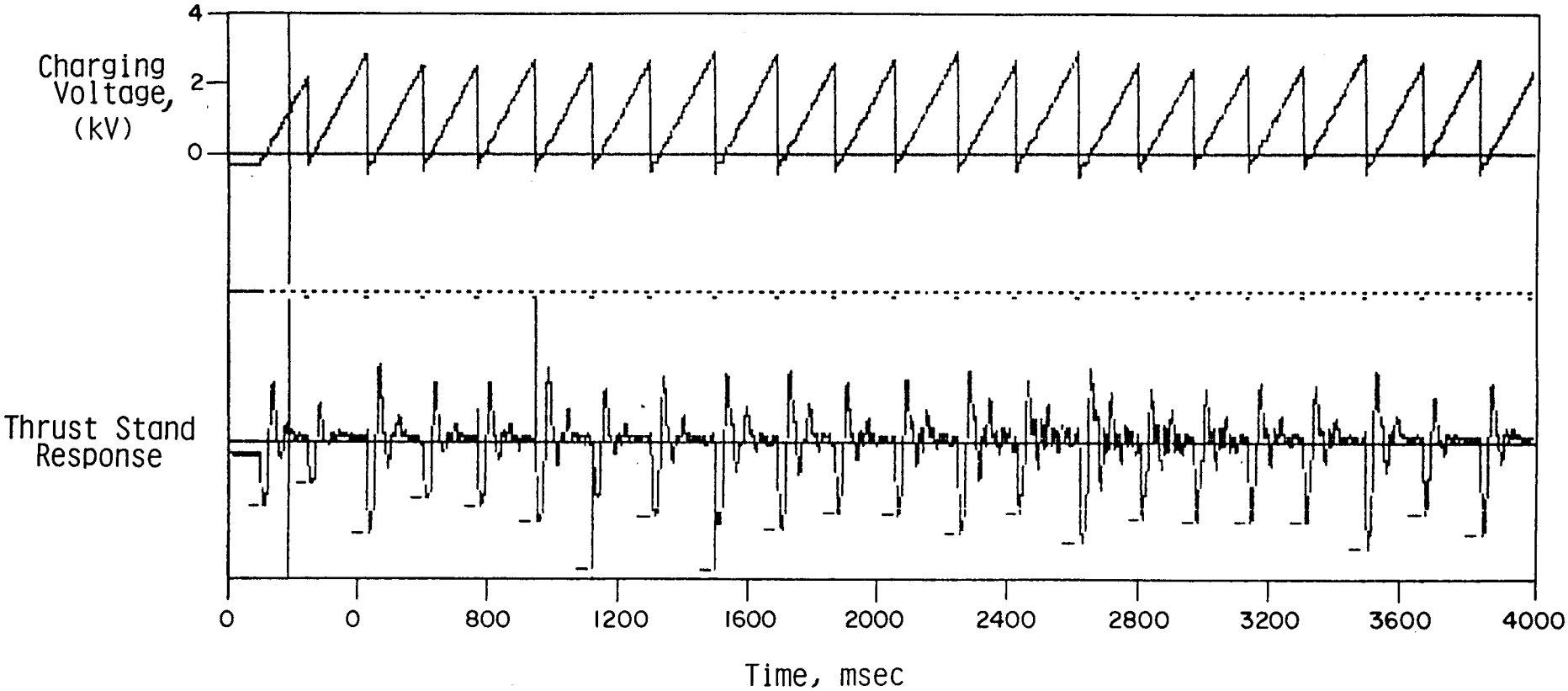

Figure 4. TYPICAL PET THRUSTER RUN, SHOWING SHOT-TO-SHOT VARIATION IN VOLTAGE (UPPER) AND THRUST (LOWER)

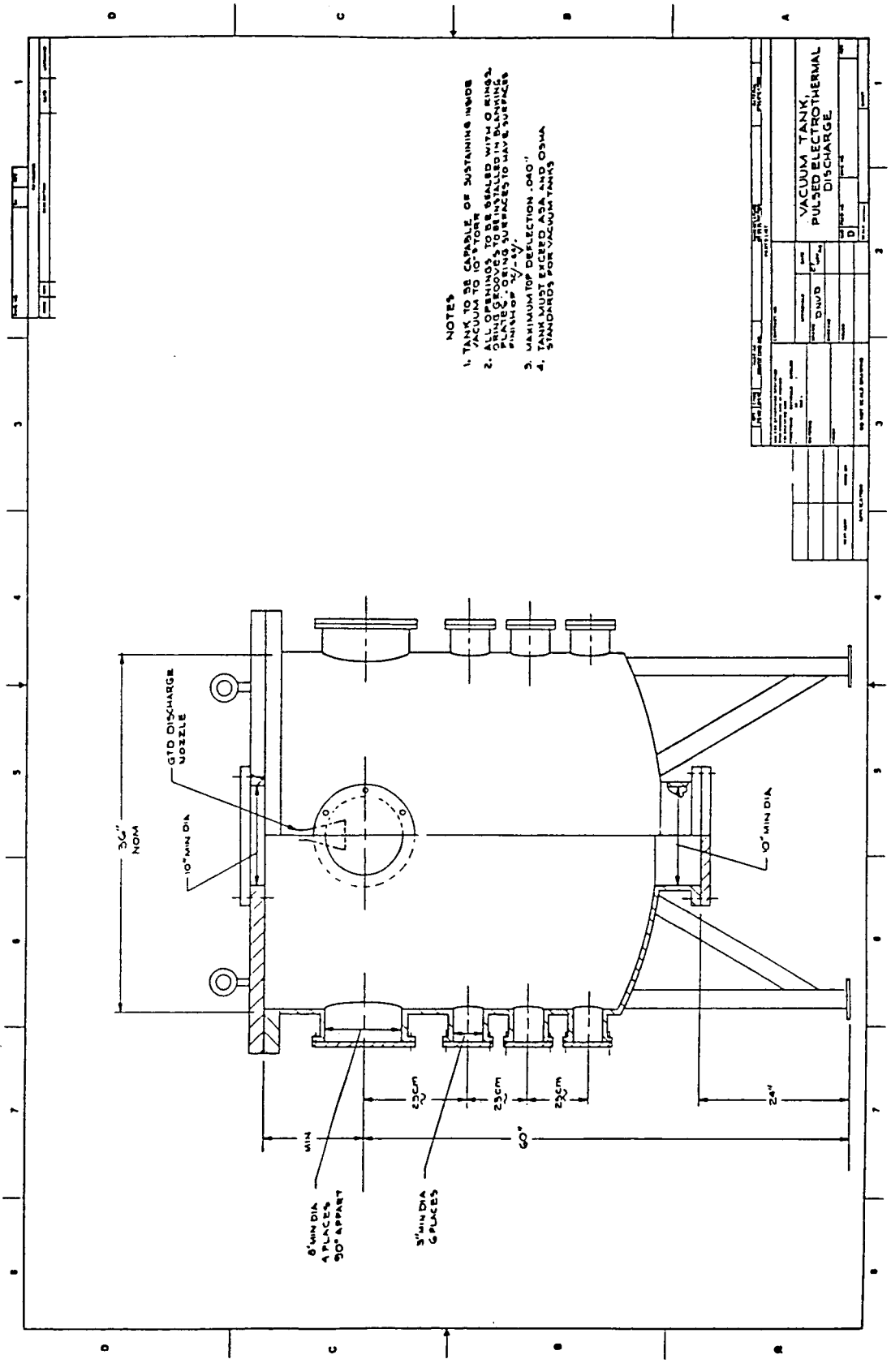

Figure 5. EXPERIMENTAL VACUUM TANK

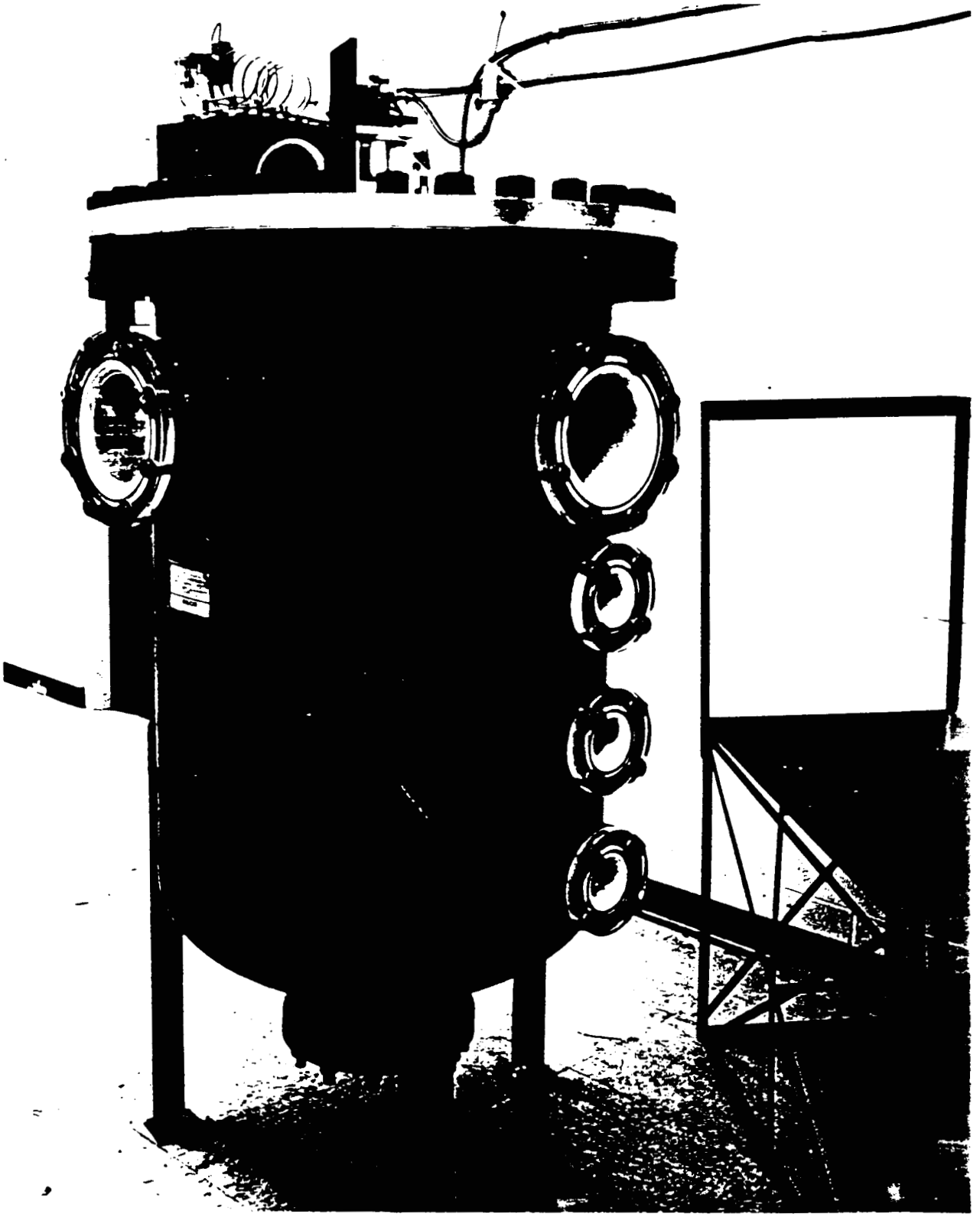

Figure 6. VACUUM TANK WITH
PET THRUST STAND AND PFN

and when the current is time-integrated, gives good agreement with the charge on the bank. Thrust impulse is detected on a thrust stand, calibrated with a pendulum (Fig. 7) [2]. The stand is operated with the axis vertical, and is relatively friction free, typically executing five half cycles after each impulse (Fig. 8). The recoil motion is detected with a highly linear inductive transducer (Bently-Nevada 7200 series Proximitor) which produces 8.00 V/mm opposed to an AISI 4140 steel target. The position-time (x-t) signal is differentiated graphically to give the recoil velocity, typically a few millimeters/second. The resulting recoil agrees with the calibration pendulum to within 1.5% [2].

Previous PET thruster measurements [1-2] were taken at the 2000 joule/discharge level, and resulted in high thrust stand signal to noise ratio. For repetitive operation only tens of joules are available for the discharge, and thrust stand signal to noise ratio was of some concern. Fortunately, the thrust stand design was capable of operating at two orders of magnitude less signal, although a small megahertz level noise signal was induced by the Proximitor. This signal was of sufficiently higher frequency than that of the thrust stand natural frequency (20 Hz) that it could be easily filtered out with a .05 μf capacitor across the Proximitor output. A typical resulting signal is shown in Figure 8.

The primary design problem for repetitive operation is the water injection nozzle. The quantity of water desired for each

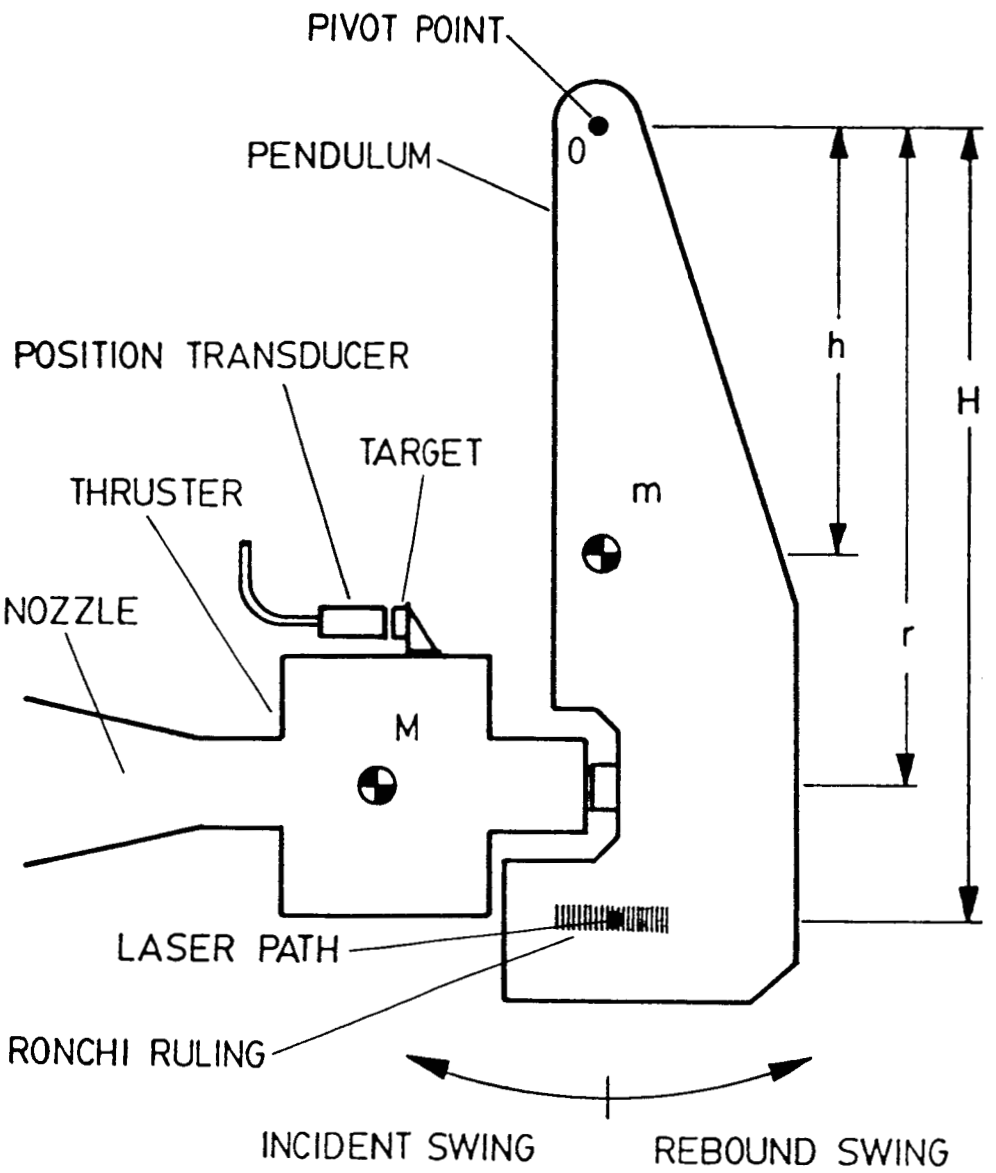

Figure 7a. THRUST STAND CALIBRATOR SCHEMATIC

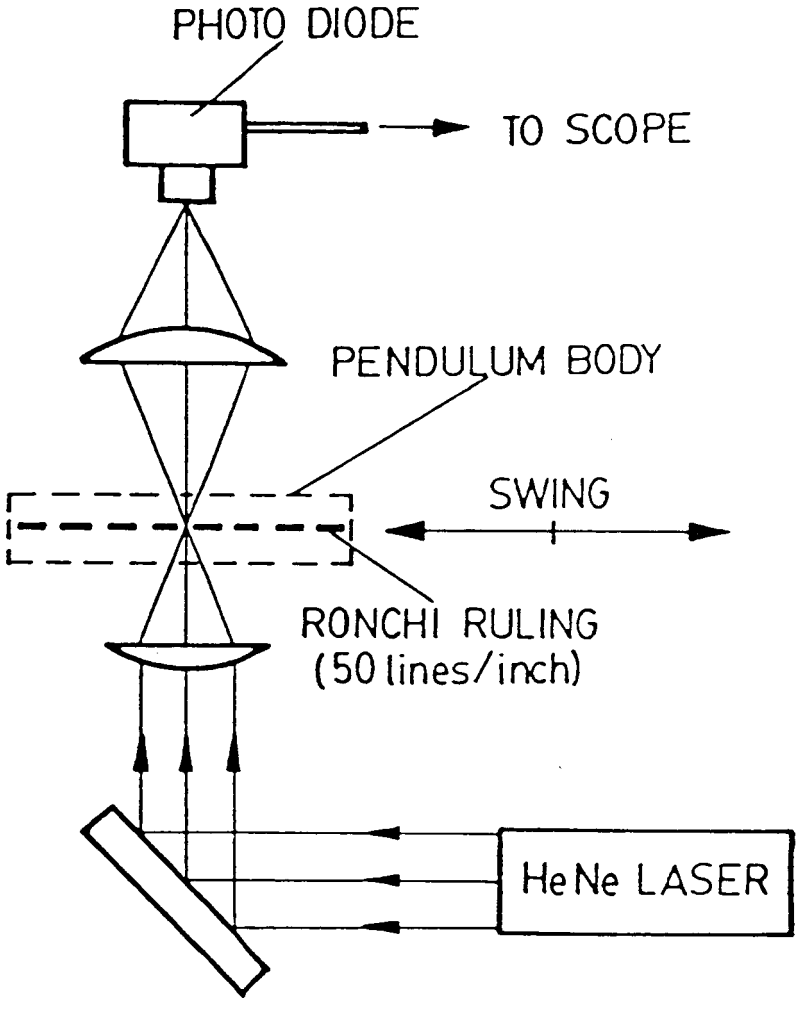

Figure 7b. CALIBRATOR OPTICAL SCHEMATIC

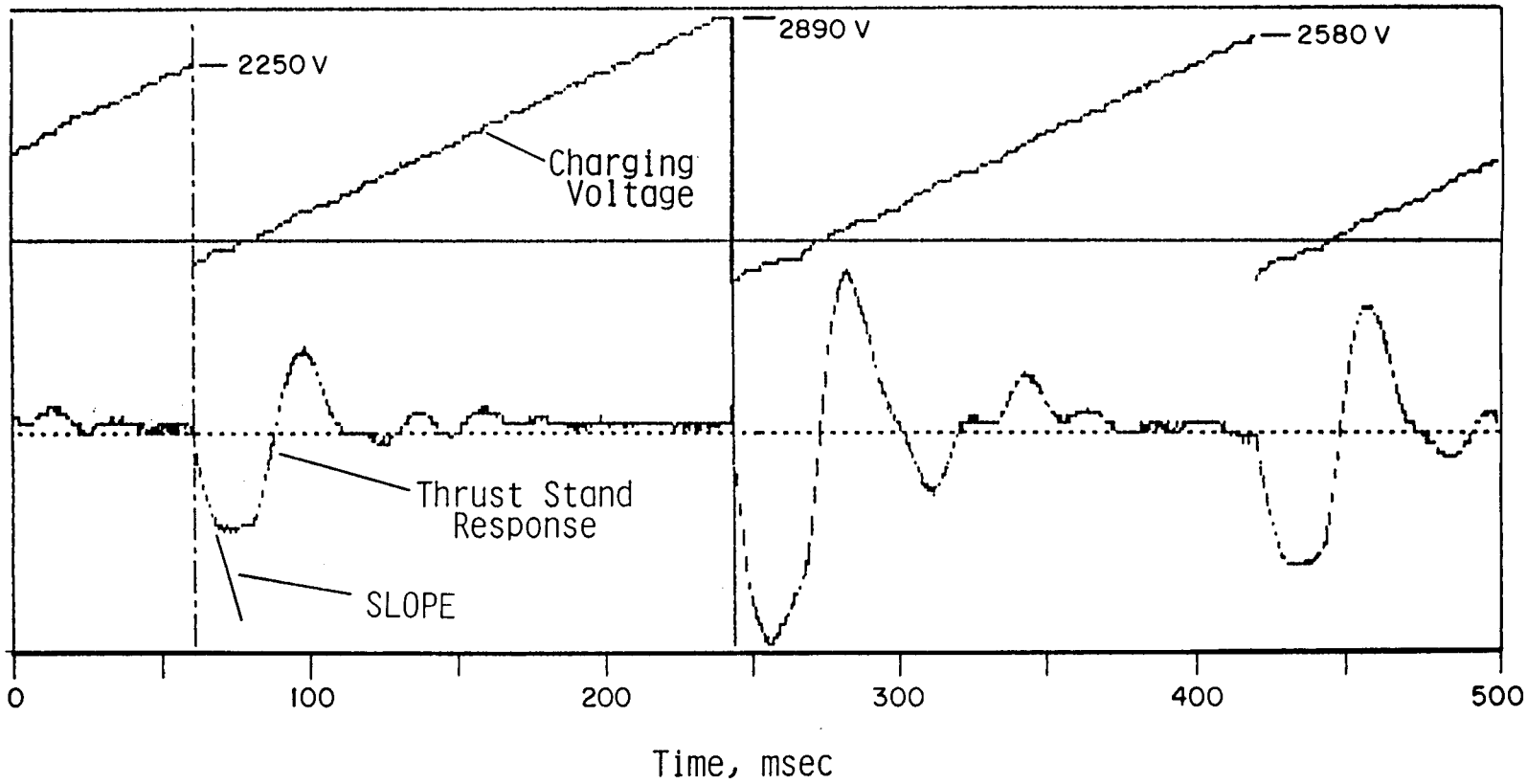

Figure 8. THRUST STAND RESPONSE TO THRUST IMPULSE

discharge is calculated for a typical discharge energy of 40 J and the water enthalpy, which for a typical temperature of 1.8 eV is 160 J/mg. The mass per discharge is then .25 mg, or .25 mm^3 of water. At 500 watts the discharge rate 12.5 Hz, giving a volume flow of 3.1 mm^3/sec. The flow velocity through the injection nozzle is then 18 cm/sec, for a typical injector ID of .15 mm. The fluid travel distance between pulses is thus 1.5 cm, which is half the capillary length of 2.8 cm. At this condition, then, the water is contained within the discharge capillary during the pulse.

There is a problem with this type of injection scheme however, caused by the viscosity of the water. Instead of forming a fluid jet, the water at these low velocities forms a small drop, which grows until it breaks off gravitationally from the nozzle tip. This drop fills the discharge capillary, and causes erratic thruster operation. The solution is to increase the mass flow rate. At a critical velocity estimated to be 150 cm/sec, the water does indeed form a jet. It is this latter mode in which the experiments are run.

In order to achieve an injected jet then, instead of a droplet, the thruster is overfed by a factor of actual velocity (150 cm/sec)/required velocity (18 cm/sec) = 8.3. This overfeeding is dictated by the injection orifice diameter and the available power. Reducing the orifice area by a factor of 8.3 or increasing the power by a factor of 8.3 would consume all the injected water. These strategies were not available during the present

investigation, due to the limited size of the power supply and the unavailability of smaller orifices.

The thruster was tested with four injection nozzle designs. These were:

1. A drafting pen tip, .15 mm inner diameter, located 1.8 cm back from the tip of the injector electrode, fed by a water metering gauge.

2. An annular nozzle created by a .343 mm pin (#80 drill) in a .368 mm hole, located flush with the tip of the electrode, with no water metering gauge.

3. The same design as 2., but with the injector orifice recessed 3 mm from the tip of the electrode.

4. The same design as 3., but with the pin removed.

Discussion of injection system designs

1. The drafting pen tip produced an erratic flow, due to the large distance (1.8 cm) from the electrode tip. The injected flow would sometimes fall cleanly down the axis of the thruster, and would sometimes cling to the side of the discharge capillary. Voltage variations of 2:1 were observed. A second problem was caused by the variable area flow metering valve (GILMONT #1) which was located between the water reservoir and the nozzle. The reduced pressure in the feed-line caused bubble formation so that the flow rate varied considerably, and was not reproducible. This design did not prove practical and was abandoned.

2. The annular nozzle with pin and no water metering gauge put the pressure drop at the orifice, which was good. This nozzle formed drops, however, and due to the high surface area could not be forced into a jet mode. An additional problem was the blowback of tungsten electrode material into the gap (only 12.5 microns), which caused clogging of the nozzle.

3. Recessing the annular orifice 3 mm from the tip solved the clogging problem but not the droplet problem. This design was therefore rejected.

4. Removing the central pin produced a workable nozzle, without clogging, droplet formation, or clinging to the wall. This design did cause the thruster to be overfed, so that not all the propellant was evaporated by the discharge. This can be overcome principally by raising the thruster power level into the kilowatt range, an option which was not available for this investigation.

The nozzle design with the central pin removed was used for the performance measurements in this study, and is shown in Fig. 9.

Discharge - fluid Coupling

Because of the small size (2.5 mm dia. x 2.8 cm length) of the discharge capillary, it is not possible to observe the dynamics of the water jet during the discharge pulse. Prior to the pulse the injected water Reynolds number $\rho VL/\mu$ is 2×10^4, so the jet is presumably turbulent and starting to break up into drops. As the pulse begins the discharge power increases to several megawatts in a few microseconds, heating the water vapor surrounding the jet and

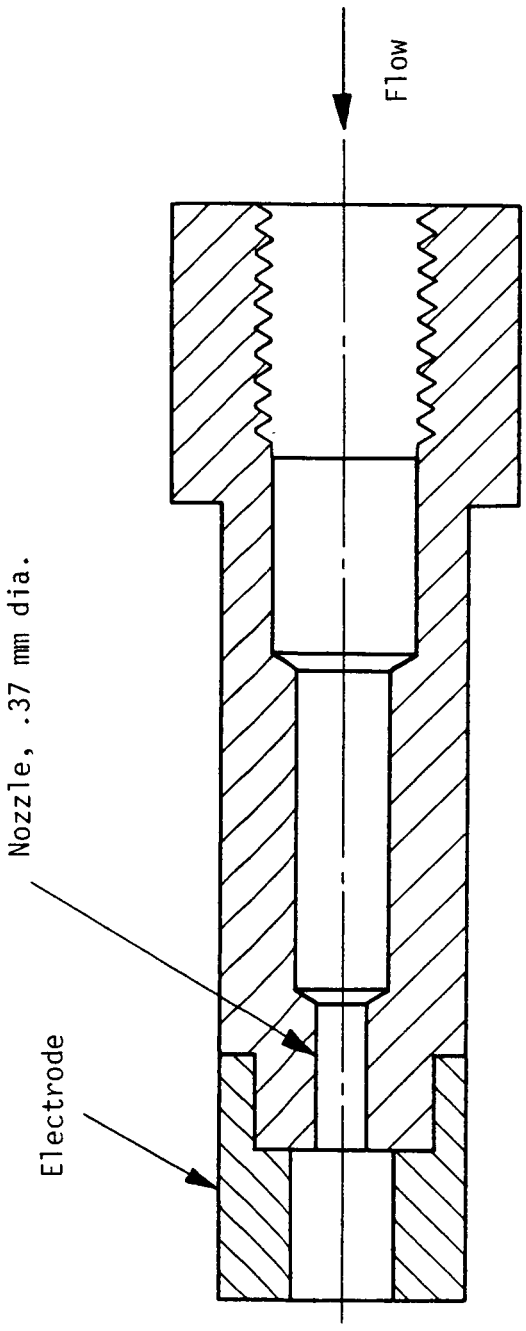

Figure 9. WATER INJECTION ELECTRODE

driving it toward the throat to a sonic velocity of about 6 km/sec. At the same time, the capillary pressure increases to a few hundred atmospheres (several thousand psi) with a strong axial gradient, and the temperature increases to 20,000 K, producing a blackbody radiation flux of over one megawatt/cm^2. It might be presumed that under these harsh conditions the jet would not maintain its integrity and would break up into fine drops. The experimental evidence suggests that this is indeed the case, as is discusseed in Section III.

This point is important, because if the discharge does not cause the water to atomize, the water remains in a largely liquid form. The discharge energy would then ignore the liquid and heat the small amount of vapor present to much higher temperatures (30,000-50,000 K), so that the discharge energy would be lost in radiation to the walls. The high radiation flux would then ablate the walls, and the thruster walls would erode away in a few thousand pulses.

Another consideration of repetitive operation is possible interruption of the water injection process by the discharge. The water is injected from a source at 1 atm pressure, p_o, into a near vacuum (a few torr). During the discharge the pressure rises to 200 atm, p, for 12 microseconds. This reduces the momentum of the incoming water by an amount proportional to $pt_p = (200)(12) = 2400$. This momentum loss is then recovered in a time given by $t_R = pt_p/p_o$ = 2400 microseconds. Since the time between pulses at 12.5 Hz is

80 msec, the injection flow has time to recover and is not at all disturbed by the previous discharge.

Water cooling is provided on the thrust stand, primarily to project the thruster o-rings (Fig. 2). The amount of heating is small, however. The capillary surface area is $\pi DL = 2.3\ cm^2$, and because of the boundary layer temperature profile [5], the wall radiation flux is about half the core flux, or 0.5 megawatt/cm^2. The total energy hitting the wall in 12 microseconds is thus (2.3)(.5)(12) = 14 joules. Perhaps 80%-90% of this 14 joules heats water which is wetting the surface, while the remaining 10-20% soaks into the insulator. At 12.5 Hz, the heat flux into the insulator which must be removed by cooling is 17-34 watts, or about 3-7% of the input power. Thus, for experimental runs lasting a minute or less the cooling is not necessary.

To conclude this section on repetitive operation we discuss the problem of ambient background pressure. The primary reason for requiring low background pressure is to allow time-of-flight exhaust velocity measurements. The condition required for the measurement is that the background mass be small compared to the exhaust mass, which is typically .25 milligrams as discussed above.

In previous experiments at 2000 joules discharge energy, it was not difficult to keep the background mass at less than 1% of the exhaust mass. In the present experiment, however, the discharge mass is reduced by a factor of 16 and the background

pressure increased by a factor of 10. Calculation of the ambient mass inside the 1000:1 area ratio nozzle gives an order of magnitude more ambient mass than discharge mass at a typical pressure of .01 atm.

Because of the high background mass, time-of-flight velocity measurements were not attempted. [Cryogenic pumping would have been required to attempt this diagnostic, and was unfortunately beyond the resources available to the experiment.] It is also likely that the background mass degrades thruster performance, as discussed below. Because of experimental limitations, the effect of background pressure on thrust was not investigated in this experiment.

III. PET THRUSTER MEASURED PERFORMANCE

The PET thruster performance was documented for a total of seven runs (Runs 11-17), which are summarized below in Table I. These runs, which were performed without changing the thruster hardware, used the injector electrode nozzle shown in Figure 9.

Table I. PET Thruster Performance Runs

Run	P.S. Current	Rep. Rate	Approx. E/Pulse	Mean Power	Est. Total Pulses	Est. Total Energy
Development*	-	-	50J	100W	400	20 kJ
11	73 mA	2 Hz	40	80	200	8
12	73	2	50	100	100	5
13	73	2	50	100	100	5
14	490	9	70	630	4	0
15	490	10	60	600	4	0
16	270	6	60	360	300	12
17	340	9	50	450	300	15
					1400	65 kJ

*Data lost

Runs 11-13 were at relatively low power (100 watts). Runs 14-15 were at the maximum power available (600 watts), but overloaded the power supply (400 watts).

Three channels of data were recorded for each run: discharge voltage, discharge current and thrust stand response. Data was recorded digitally on a Soltec Signal Memory Recorder at two different sample rates, 2 megahertz and 2 kilohertz. The scope is triggered on the falling signal from the thruster discharge voltage on the first pulse. The scope captures 2000 data samples before triggering and 3000 data samples after triggering at the 2 megahertz rate, which provides good time resolution for the voltage and current history of the first pulse. The scope then switches to a 2 kilohertz rate, and captures 11,000 points (5.5 sec) worth of data at the slower rate, to resolve the charging voltage and thrust stand response for several consecutive pulses.

The discharge voltage and current time histories for the first pulse are shown for Runs 11-13 in Fig. 10. The zero to zero current pulse length is 16 microseconds. The FWHM length is 12 microseconds. The DC voltage level at negative time gives the bank charging voltage. The product of V and I when integrated over the pulse gives the energy transferred to the discharge, as is discussed below.

The voltage, current and thrust stand response are shown in Figs. 11-17 for Runs 11-17. The repeatability of the discharge voltage can be observed in each case. In all cases the discharge voltage is observed to fall from an initial value of 2-3 kV to a negative value of a few hundred volts. This is a consequence of

Run 11

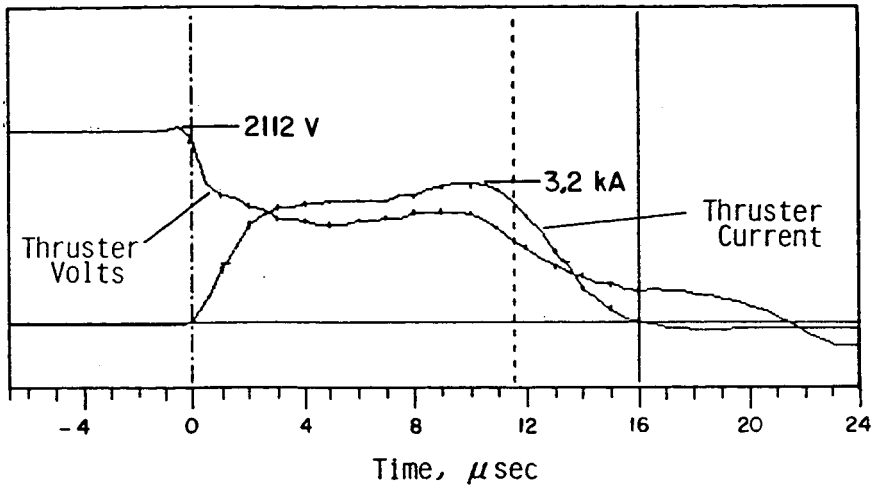

Run 12

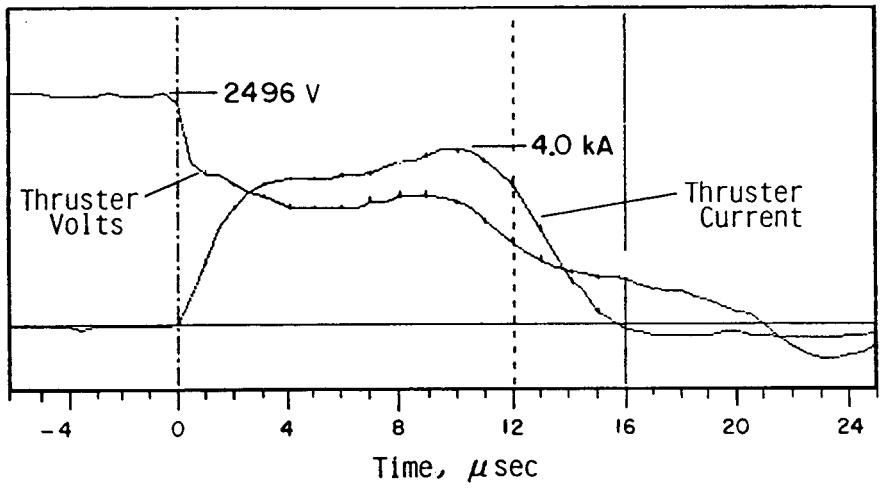

Run 13

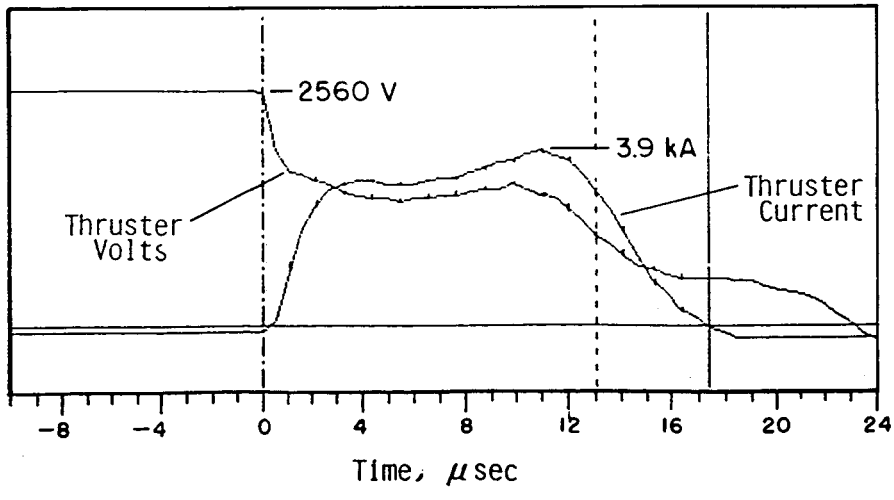

Figure 10. VOLTAGE AND CURRENT TIME HISTORIES, RUNS 11-13

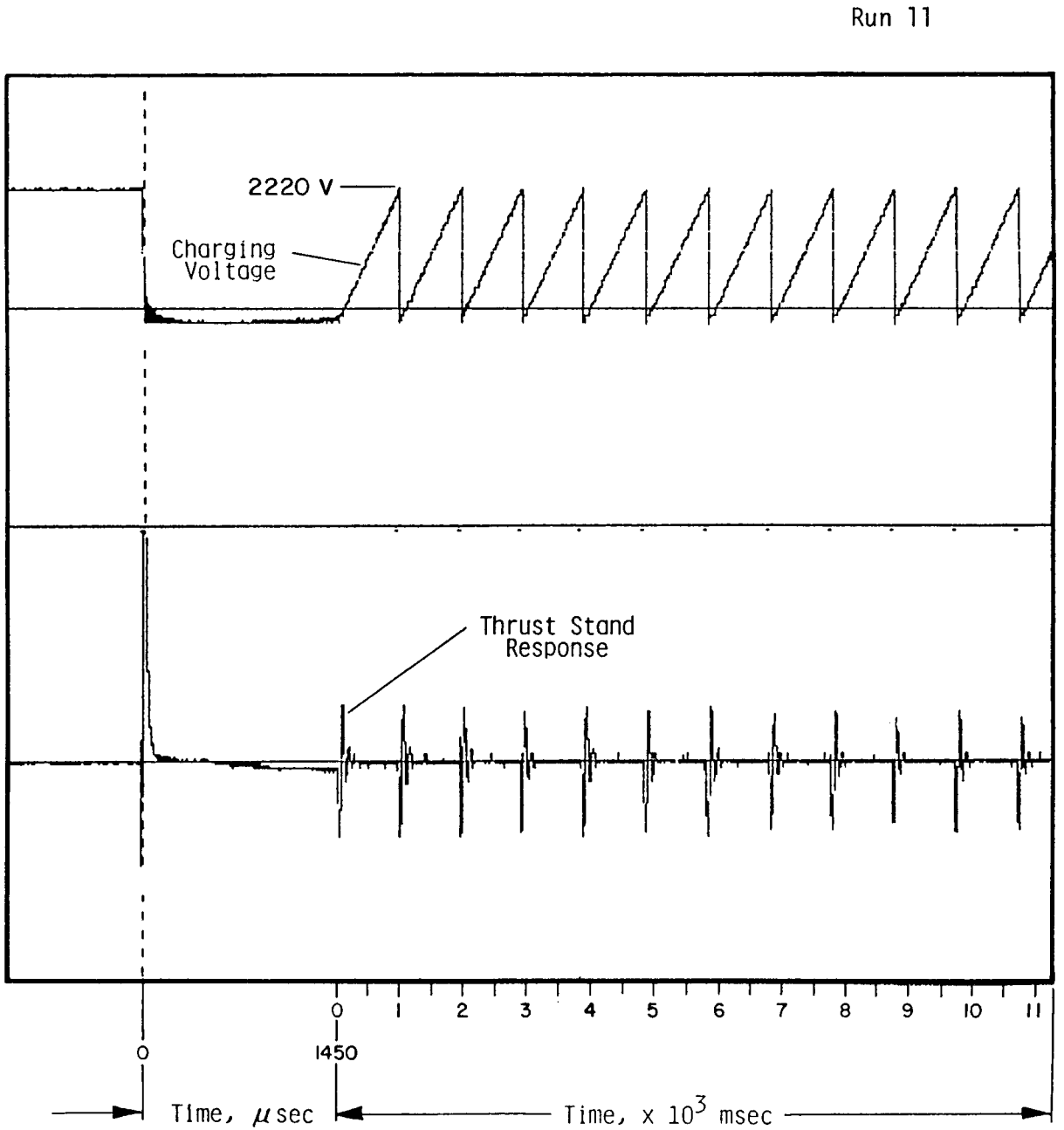

Figure 11. CHARGING VOLTAGE AND THRUST STAND RESPONSE

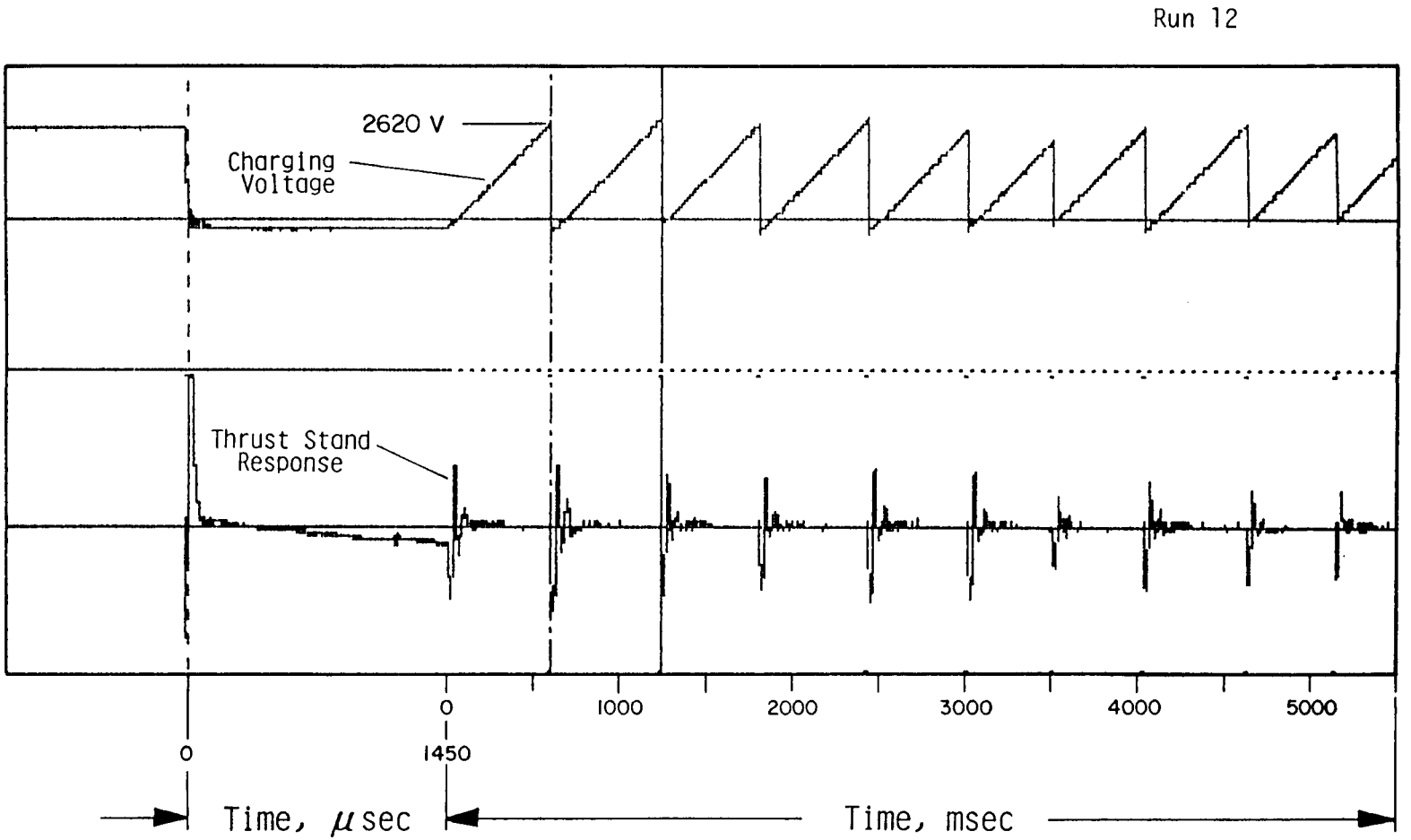

Figure 12. CHARGING VOLTAGE AND THRUST STAND RESPONSE

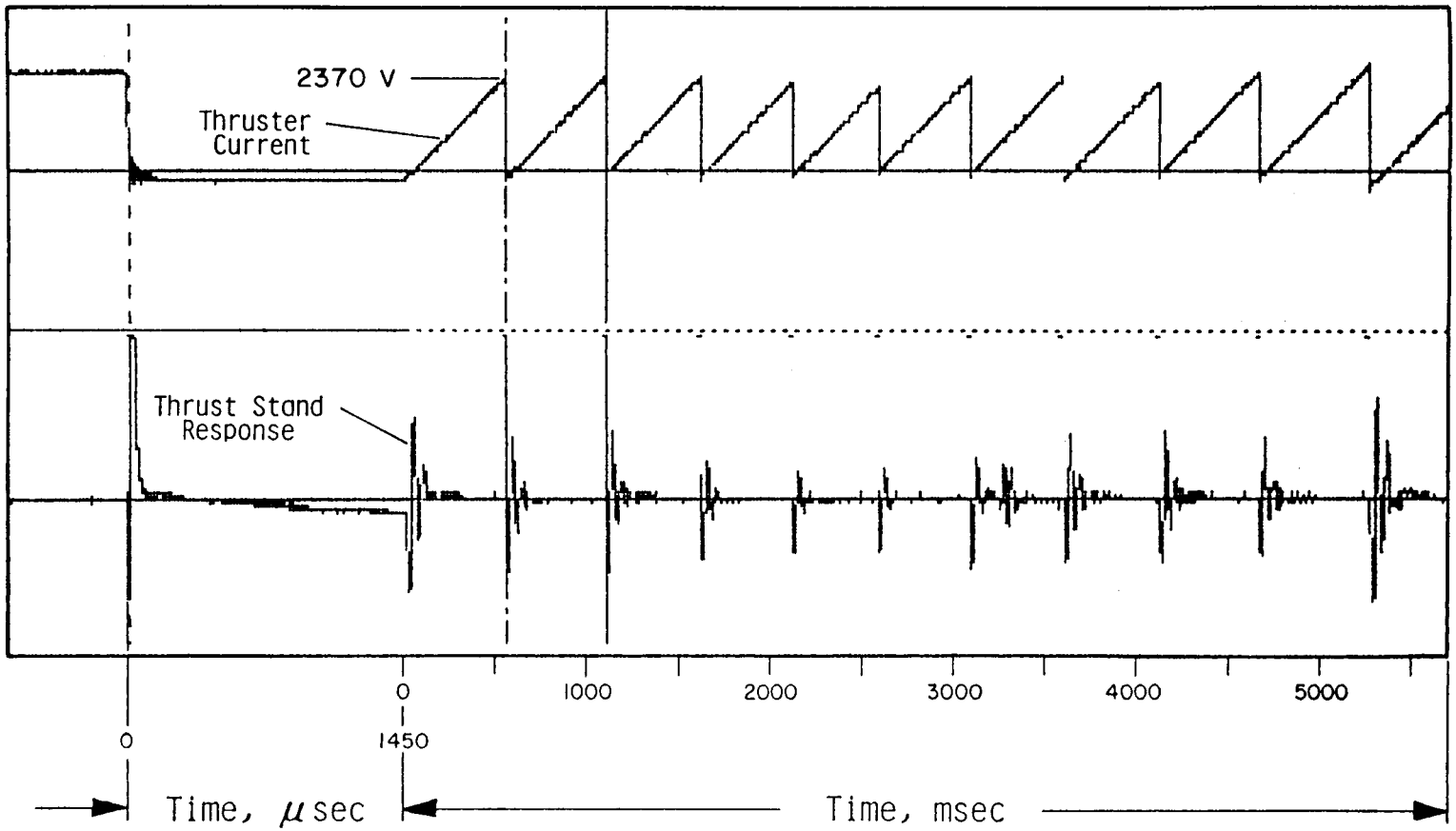

Figure 13. CHARGING VOLTAGE AND THRUST STAND RESPONSE

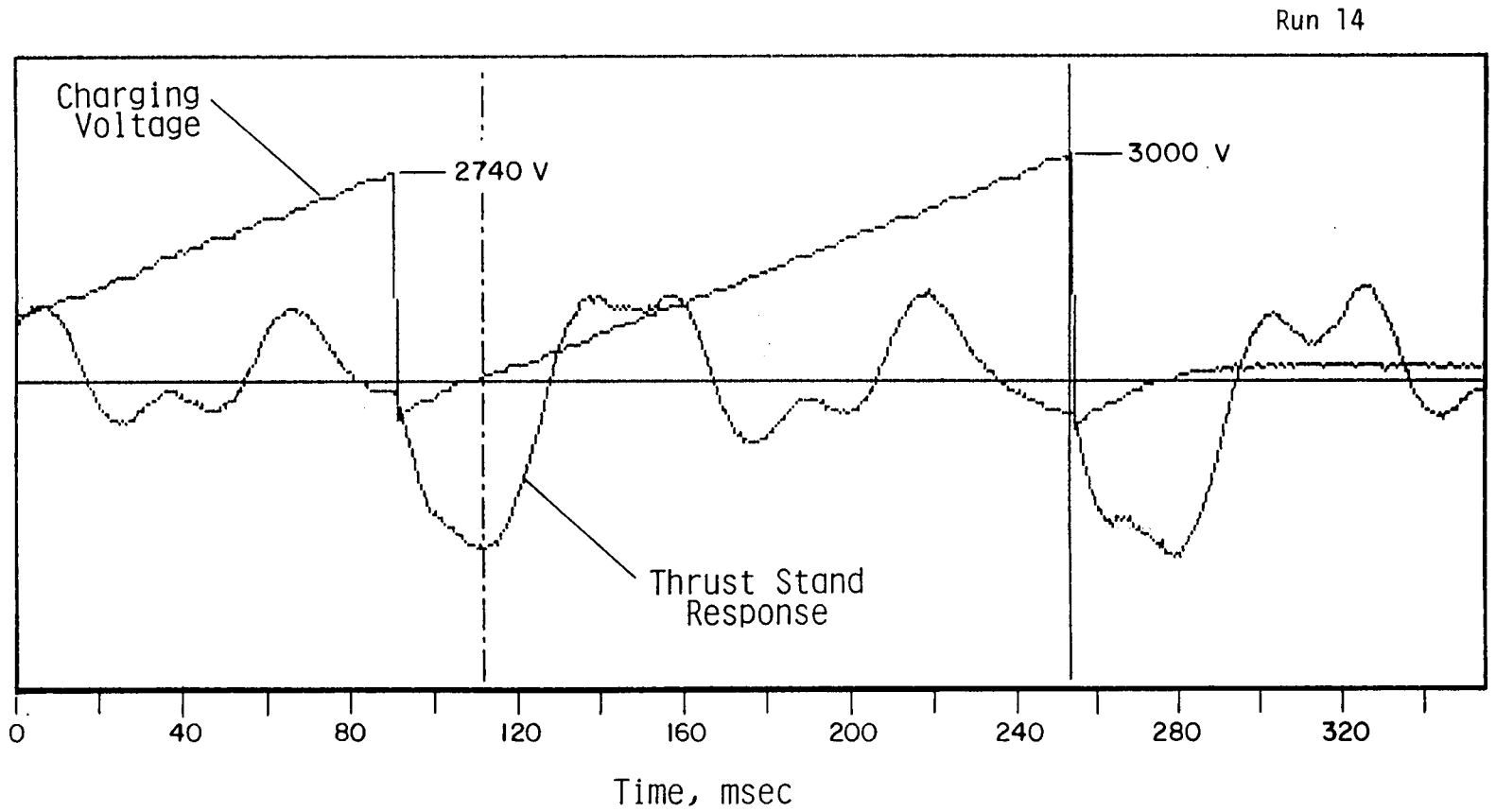

Figure 14. CHARGING VOLTAGE AND THRUST STAND RESPONSE

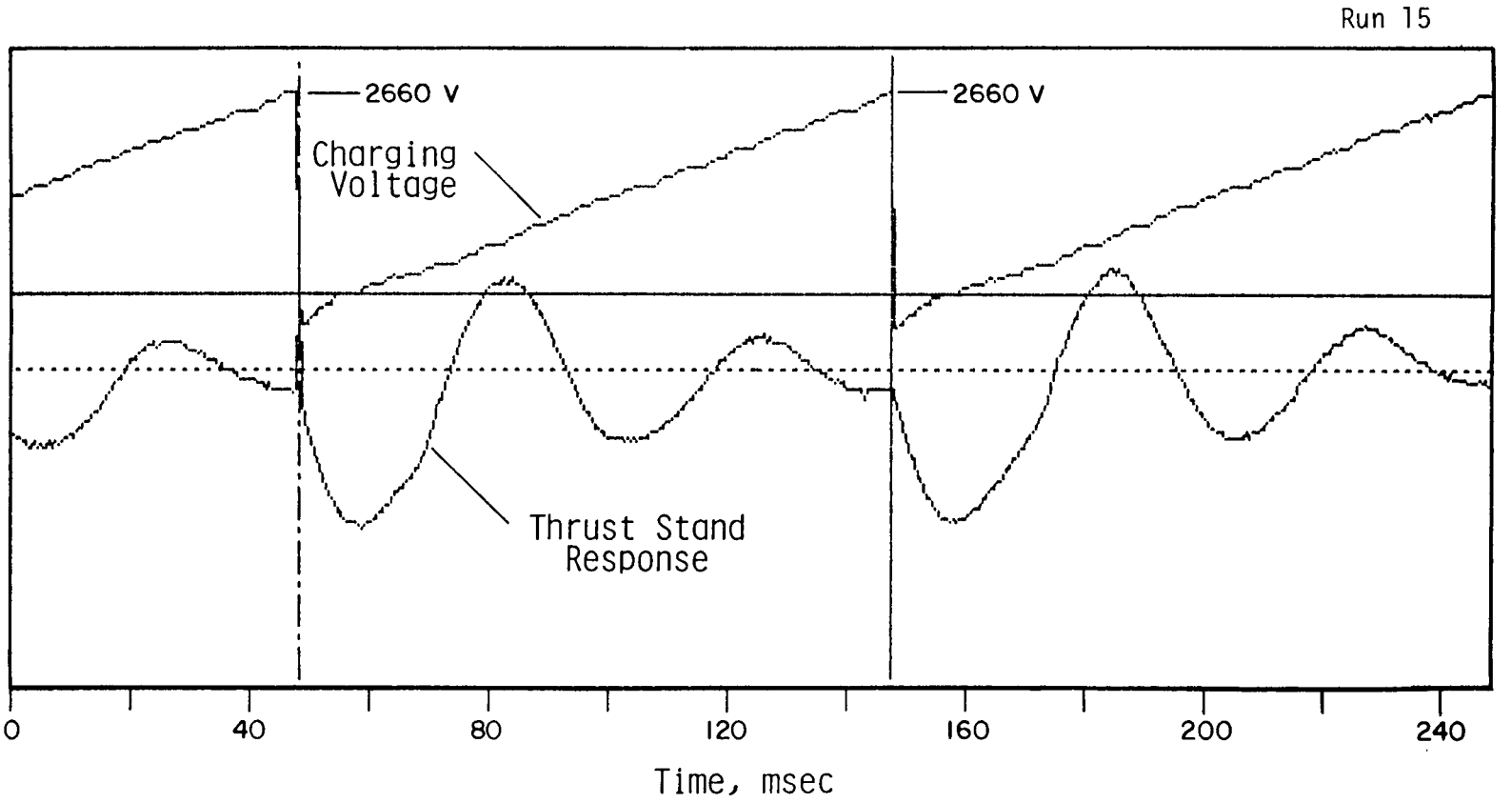

Figure 15. CHARGING VOLTAGE AND THRUST STAND RESPONSE

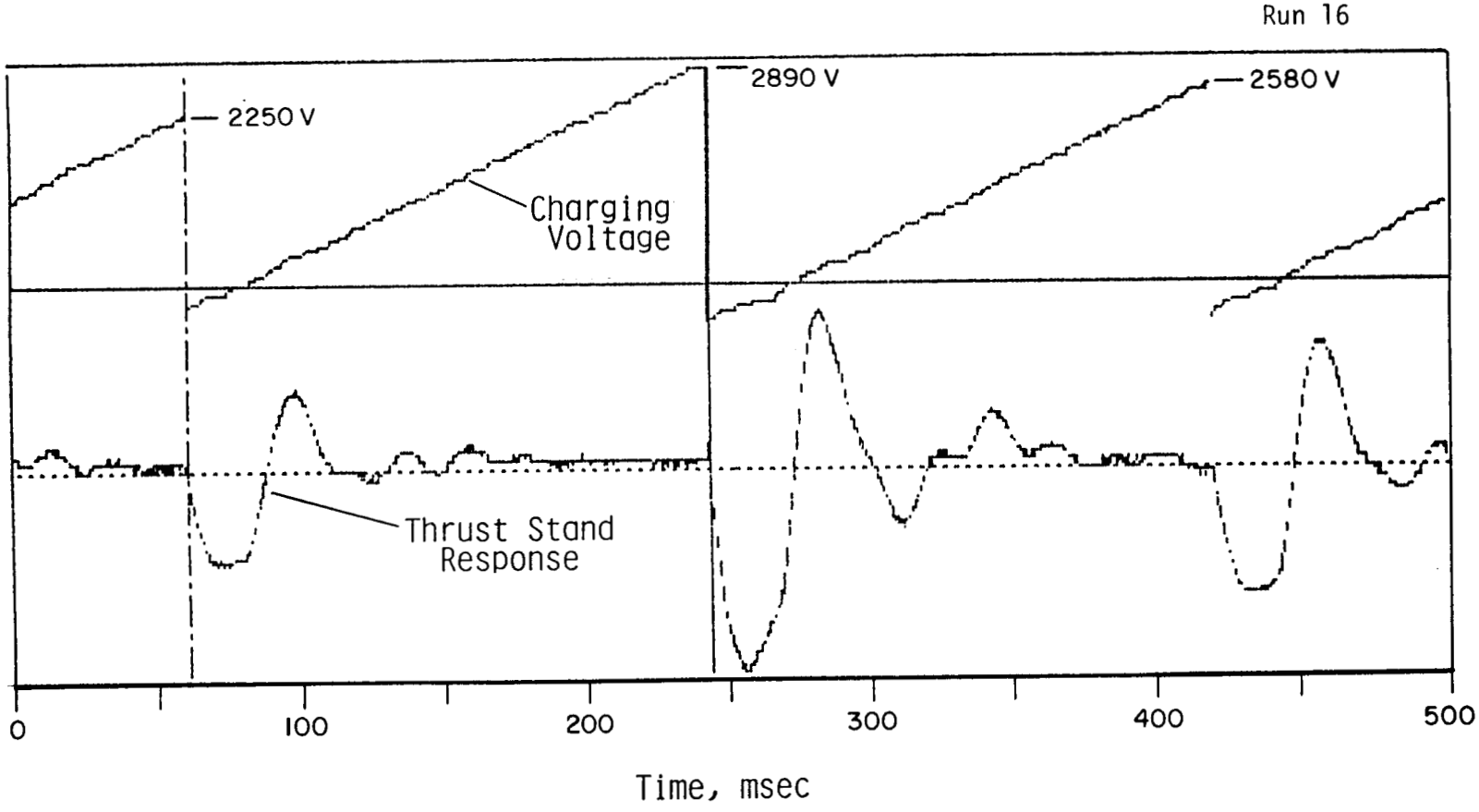

Figure 16. CHARGING VOLTAGE AND THRUST STAND RESPONSE

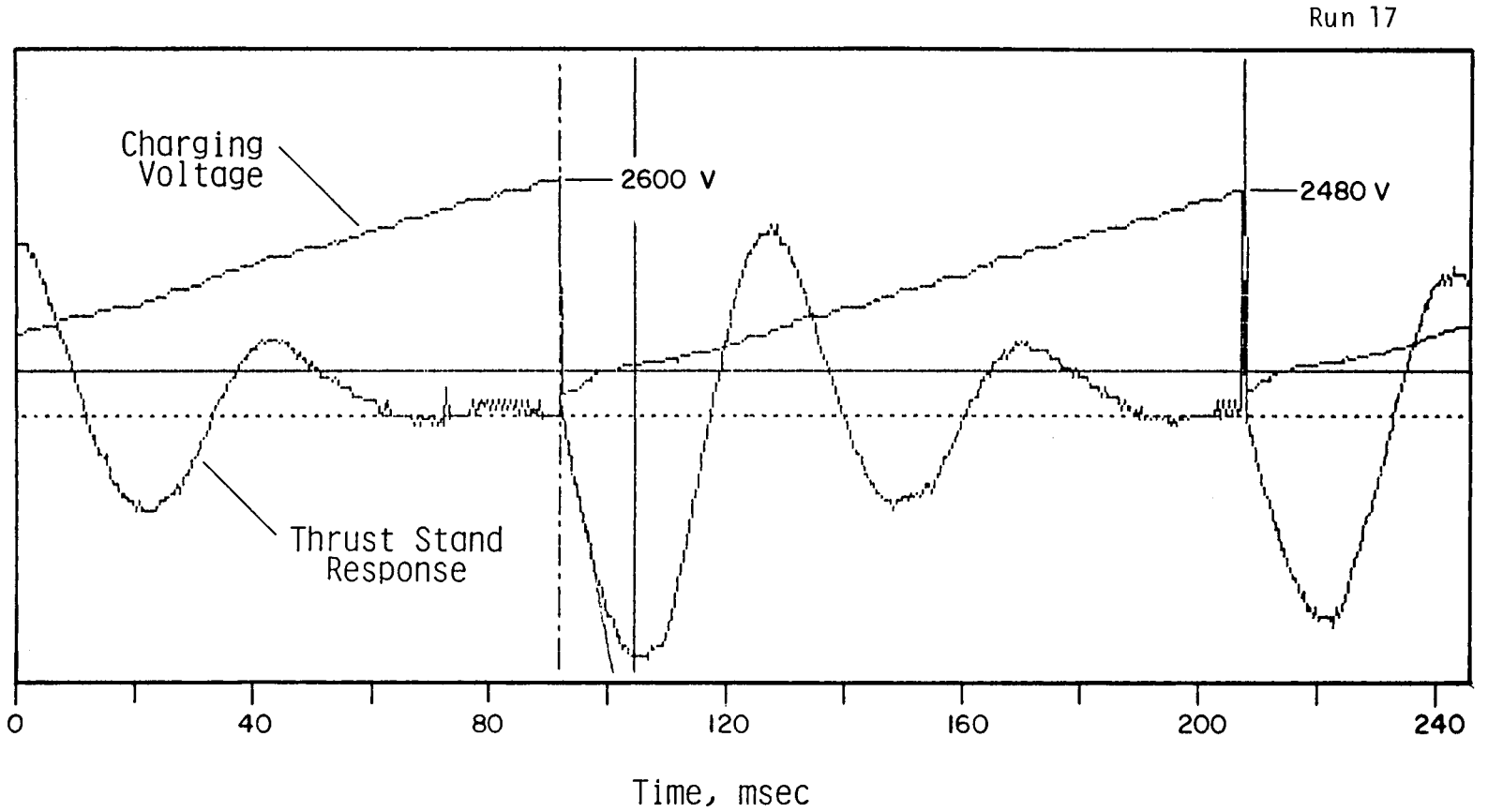

Figure 17. CHARGING VOLTAGE AND THRUST STAND RESPONSE

the thruster being directly attached to the capacitor bank. When the discharge power is insufficient to ionize the water the thruster acts as an opening switch. The discharge current is never observed to reverse, and the thruster always opens with a small reverse voltage on the bank. This reverse voltage is small enough that the cycle life of the 8 kV capacitors should not be significantly affected.

The initial slope of the thrust stand x-t response is an exact measure of the recoil velocity, but the amplitude of the first negative peak is a more readily visualized indicator of this velocity. These amplitudes and their shot-to-shot variation can be observed in Figs. 11-17. It should be noted that the mean value holds relatively constant when averaged over any consecutive ten discharges.

Data Analysis

The thrust-to-power ratio is:

$$\frac{T}{P} = \frac{\int T dt}{\int P dt} = \frac{\text{impulse bit}}{\text{stored energy}}$$

The impulse bit is measured by the thrust stand, and the stored energy by the capacitance and bank voltage. It is more correct to define T/P as impulse bit/delivered energy, but delivered energy and stored energy are nearly equal, as has been discussed. Values of T/P for the first pulse in each run are shown below in Table II.

Table II. Samples of T/P from Runs 11-17

Run	First Impulse Bit	$1/2\ CV_o^2$	T/P
11	2.8 mN-sec	35J	.079 N/kW
12	4.2	50	.083
13	4.1	52	.077
14	5.4	68	.079
15	3.6	58	.063
16	3.8	58	.065
17	2.8	51	.062
		Mean	.073 N/kW

Table II gives a mean T/P of .073 N/kW for Runs 11-17. Although the power level in these runs varies from 100-600 watts, this is accomplished solely by varying the pulse rate, so that it is meaningful to compare T/P at different power levels.

Next we analyze some individual pulses (Fig. 10). The voltage probe (Tektronix P6015) is calibrated at 1000:1 with a pulse generator. The capacitance of the bank is checked on a bridge, and agrees with the manufacturer's specification of 16 microfarads. The Rogowski coil with 2.8 msec passive RC integrator is calibrated by two different techniques; by comparison to a current transformer and by comparing $\int I dt$ with the known charge on the capacitors. Both techniques give 104 kA/V. The pulses are then analyzed at 1 microsecond intervals for Runs 11-14. The results are shown in

Figure 18. A condensation of the results is shown in Table III below.

Table III. Measured Pulse Conditions, Runs 11-14

	Run 11	Run 12	Run 13	Run 14
Bank V_o, kV	2.11	2.50	2.56	2.91
Bank energy, J	36	50	52	68
Discharge Voltage, kV	1.13	1.35	1.45	1.55
Discharge Current, kA	2.78	3.37	3.35	3.98
Discharge Power, MW	3.1	4.5	4.9	6.2
Discharge Energy, J	35	50	54	68
Discharge Resistance, Ω	.40	.41	.44	.39
Impulse Bit, mN-sec	2.8	4.2	4.1	5.4

Discussion of Data

In Figure 18, the time range from 3 to 11 microseconds is referred to as the flattop region, where the voltage and current vary relatively slowly. In particular, the last row in each run gives the discharge resistance in the flattop region, V/I[ohms]. It can be seen (Fig. 18) that the resistance varies very little over this time period. This result had not been expected, as it

Figure 18. DISCHARGE PULSE, RUNS 11-14

t, μsec	0	1	2	3	4	5	6	7	8	9	10	11	12	13	14	15	16
Run 11					← Flattop Regions →												
V, kV	2.02	1.37	1.24	1.11	1.08	1.03	1.08	1.10	1.15	1.17	1.15	1.02	.81	.62	.51	.42	.54
I, kA	0	1.13	2.13	2.50	2.64	2.67	2.67	2.67	2.79	2.93	2.96	2.92	2.37	1.55	.71	.27	.2
VI, MW	0	1.55	2.64	2.78	2.85	2.75	2.88	2.94	3.21	3.50	3.52	2.97	1.92	.98	.3	.14	0
V/I, Ω*	—	1.21	.58	.44	.41	.39	.40	.41	.41	.39	.38	.35	.34	.39	.72	1.57	—
Run 12																	
V, kV	3.42	1.66	.56	.40	.37	.37	.37	.33	.39	.39	.34	.15	.09	.08	.07	.07	.07
I, kA	0	1.35	2.49	2.98	3.11	3.1	3.11	3.23	3.48	3.57	3.75	3.42	2.97	2.03	.97	.39	0
VI, MW	0	2.24	3.81	4.	3.97	3.95	4.04	4.30	4.14	4.96	5.10	4.05	2.64	1.42	.5	.1	—
V/I, Ω*	—	1.23	.63	.47	.41	.41	.41	.42	.41	.40	.36	.33	.30	.35	.63	1.7	—
Run 13																	
V, kV	3.52	1.66	.57	1.45	1.39	1.34	1.39	1.40	1.47	1.54	1.42	1.27	.91	.77	.62	.4	.4
I, kA	0	1.35	2.63	3.10	3.18	3.12	3.16	3.25	3.41	3.58	3.87	3.59	2.98	2.17	1.22	.47	.1
VI, MW	0	2.24	4.13	4.50	4.42	4.18	4.39	4.56	5.01	5.51	5.41	4.56	2.77	1.64	.68	.19	.1
V/I, Ω*	—	1.23	.61	.47	.44	.43	.44	.44	.44	.44	.37	.35	.33	.36	.58	1.2	—
Run 14																	
V, kV	2.71	1.92	1.77	1.55	1.49	1.42	1.49	1.56	1.56	1.61	1.55	1.28	1.05	.77	.64	.5	.5
I, kA	0	1.99	3.16	3.46	3.63	3.72	3.72	3.66	4.10	4.21	4.38	3.95	3.23	2.29	1.05	.34	.2
VI, MW	0	3.51	4.9	5.0	5.4	5.3	5.51	5.58	6.4	6.79	6.8	5.11	3.39	1.76	.67	.17	0
V/I, Ω*	—	.96	.56	.45	.41	.38	.41	.40	.38	.38	.35	.32	.33	.42	.61	1.4	—

*V/I not corrected for Ld I/dt

had been assumed that the resistance would fall continuously during the pulse as the water vapor plasma was heated. This constant resistance behaviour implies instead that the discharge temperature is relatively constant throughout the pulse, which implies that two phase flow exists.

The model that best fits this data is one in which the liquid jet breaks into droplets, which then continuously evaporate to replace the heated vapor exiting from the throat. An alternate model for which the jet does not break up will not fit the data, since the surface area of the water would be too small to absorb the discharge radiation, and the temperature would be about twice as high. A second alternate, in which the liquid converts quickly to a fine mist or vapor, would imply a continuously rising temperature and dropping resistance which was not observed.

Discharge conditions are calculated from a zero-D steady state electrical/flow model[5-6], which assumes Spitzer resistivity (corrected for electron-neutral collisions) and a balance between radiation flux, evaporated water enthalpy flux, and nozzle enthalpy flux. The discharge is driven in the model by a constant impedance voltage source (the PFN). The model predicts the temperature, and the stagnation sound speed and specific heat ratio are then interpolated from the Los Alamos Sesame tables [7]. The results are shown in Table IV.

Table IV. Calculated Discharge Pressure and Temperature from Model

	Run 11	Run 12	Run 13	Run 14
Source impedance, ohms	.31	.31	.31	.31
Source voltage, kV	2.11	2.50	2.56	2.91
Vapor surface area, cm^2	3.7	5.5	6.8	7.3
$\ell n\Lambda\ (1 + 2\nu_{eo}/\nu_{ei})$	3.0	3.0	3.0	3.0
Specific heat ratio	1.20	1.20	1.20	1.20
Discharge Current, kA	2.95	3.44	3.39	4.12
Resistance (calc) ohms	.400	.412	.440	.392
Temperature, eV	1.74	1.71	1.64	1.78
Sound speed C_o, km/sec	5.8	5.8	5.7	6.0
Stagnation pressure, atm	280	400	420	520
Calc. impulse bit, mN-sec $C_F = 1.5$	4.2	6.0	6.3	7.8
Meas. impulse bit	2.8	4.2	4.1	5.4

At the bottom of Table IV are listed the calculated and measured impulse bit. The calculated impulse bit is based on the calculated pressure, throat area, thrust coefficient C_F, specific heat ratio and effective pulse length, which is the FWHM pulse length of 12 microseconds plus the one way acoustic time for emptying the capillary at the end of the pulse of 8.5 microseconds, or 20.5 microseconds:

$$\int T dt = C_F(P_e/P_o,\ A_e/A_t,\ \gamma)\ P_o A_t\ t_p$$

where C_F for steady flow is given in Ref. [8]. C_F is not known for the present case of impulsive flow in a nozzle containing an ambient fill, but has a value between 1.0 (no nozzle) and about 2.2 (infinite nozzle). A value of C_F = 1.5, appropriate for high area and pressure ratio and γ = 1.2, was adopted for Table IV, which gives calculated impulse bits about 50% higher than the measured values. Considering the approximations made, this agreement is reasonable.

Ablation

It was found more instructive to measure ablation by dimensional measurement than by mass measurement. The thruster was subjected to a number of pulses of varying energies, with an estimate of the number of pulses as 1400. The least ablation is experienced by the tungsten alloy electrodes, and the most by the boron nitride insulator.

Tungsten electrodes are located at the throat and 28 mm back at the injection orifice. Tungsten erosion is summarized in Table V. We see that the throat electrode has no measurable erosion, most probably because the throat is cooler than the stagnation region at the injector electrode. The .020 mg/shot loss from the injector electrode is caused by less than 0.1 joules/pulse being converted to hot tungsten. The total calculated radiated energy is about 1.0 joules/pulse, or ten times the amount required to cause ablation, so that the mass loss must occur at the tail end of the

pulse when the tungsten of the injector electrode reaches the melting point. A slightly shorter pulse or cooler discharge would have prevented ablation of this electrode altogetner. The throat, being cooler, never did reach the melting point.

Table V. Tungsten Alloy Erosion for 1400 Shots

	I.D.,mm		O.D.,mm		Length,mm		mass loss,mg	mass loss/pulse
	Before	After	Before	After	Before	After		
Throat Electrode	2.48	2.48	10.0	10.0	3.6	3.6	0	0
Injector Electrode	.78	.78	3.3	3.3	20.15	20.00	28	.020
							TOTAL	.020 mg/shot

Ablation of the boron nitride insulator follows a pattern consistent with the electrodes, that more ablation occurs at the injector end than at the throat end. [If the ablation were caused by convective heat transfer rather than radiation the reverse would be true. However, maximum convective heat transfer at the throat is calculated to be only 0.2 MW/cm^2, or 40% of the radiative contribution]. The insulator ablation is shown in Figure 19. The mean radial ablation is 0.36 mm, and the total mass loss is 180 mg, or .12 mg per shot. The enthalpy of heated boron nitride is 50 J/mg, so the energy absorbed by the insulator is 6 J (.12 mg/shot x 50 J/mg) out of a mean total of 60 J in the discharge. This is to be compared to the ablative wall thruster, which would have absorbed nearly all of the 60 J.

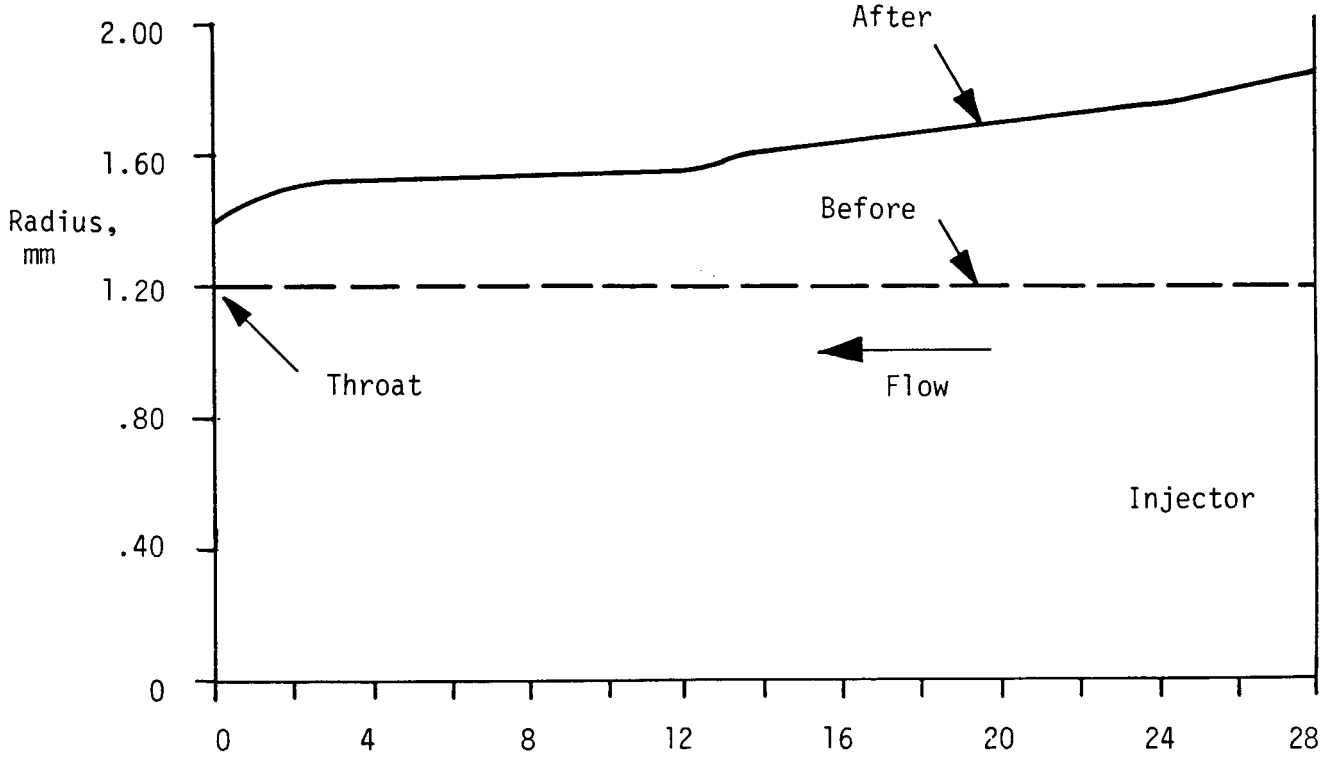

Figure 19. PET INSULATOR RADIUS INCREASE DUE TO ABLATION

If we perform a calculation similar to that for the tungsten, the total radiative energy flux to the wall during the pulse is about 13 J, so that once again it appears that the boron nitride is evaporated at the end of the pulse. A shorter pulse or cooler discharge is required to completely prevent insulator ablation.

Performance

Because of the high ambient background pressure in the tank, the exhaust velocity must be estimated. This can be done from the measured energy/pulse, calculated enthalpy, and measured impulse bit. From the calculated temperature of 1.71 $\pm$ .07 eV, the enthalpy from the Sesame tables is 168 J/mg. For Runs 11-14 where the discharge pulse was measured, we can calculate an exhaust velocity, as shown in Table VI.

Table VI. PET Thruster Performance

	Run 11	Run 12	Run 13	Run 14
Calculated temperature	1.74	1.71	1.64	1.78
Calculated enthalpy, J/mg	171	168	161	175
Discharge energy,J	35	50	54	68
Exhaust mass, mg	.20	.30	.34	.39
Meas. impulse bit, mN-s	2.8	4.2	4.1	5.4
Exhaust velocity, km/sec	14	14	12	14
Efficiency, $1/2\ U_e\ T/P$	.55	.58	.46	.55

The exhaust velocity is about 14 km/sec, which gives a specific impulse of 1400 for 100% mass utilization. The estimated uncertainty in the exhaust velocity is 15%: 5% from the impulse bit measurement and 10% from the calculated exhaust mass.

The conversion efficiency from electric to kinetic energy is given by

$$\eta = 1/2\ U_e\ T/P$$

where T/P is given in Table II. The efficiency values range from 0.46 to 0.58 with a mean value of .54, as shown in Table VI.

The exhaust velocity can also be derived from the sound speed and the nozzle expansion ratio. A steady state, adiabatic nozzle flow model, which includes the variation in the specific heat ratio γ, has been developed [9], and the predicted velocity for water as a function of area ratio is shown in Figure 20. The curve for c_o = 6 km/sec shows that an expansion ratio of only 10 is required to achieve 14 km/sec. For lower background pressure where the effective area ratio is 1000, the expected exhaust velocity increases from 14 to 17 km/sec, and the mean efficiency increases from .54 to .80.

The reason that higher velocities are not achieved is the ambient background mass, which at an area ratio of 10 is about 20% of the exhaust mass. We may hypothesize that further expansion merely entrains more ambient mass, slowing down the exhaust so that the effective nozzle ratio is not much more than 10:1.

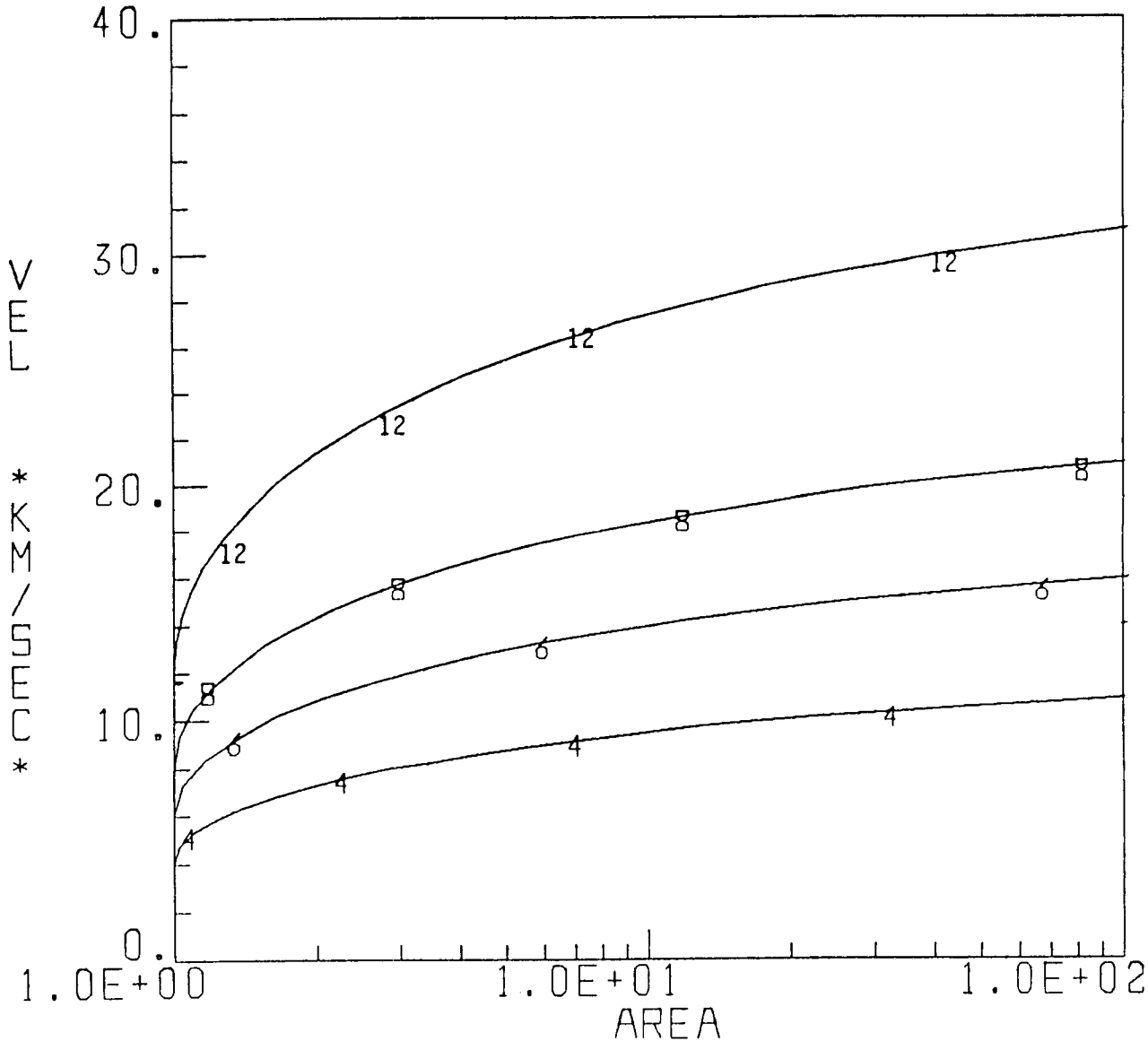

Figure 20. PLOT OF FLOW VELOCITY V VERSUS A/A_o FOR WATER, ASSUMING c_o = 12, 8, 6 AND 4 KM/SEC.

IV. CONCLUSIONS

Despite experimental difficulties with high background pressure and the injector nozzle, preliminary performance measurements have been accomplished with a repetitive PET thruster using water propellant. Operating at an overfed condition to produce an injection jet, the thruster efficiency is 54% at 1400 seconds. This is to be compared to previous results with an ablative wall thruster which gave 40% at 1500-1750 seconds. Typical thrust to power is .07 N/kW for the water-injected PET.

The principle reason that the present efficiency is higher is the reduced temperature of the discharge. The previous work with polyethylene was performed at 2.5 eV (29,000 K), whereas the present thruster is operating at 1.7 eV (20,000 K) and a comparable pressure. The recovery of dissociation energy in the water is therefore more complete, leading to better performance.

Despite the lower temperature and use of water injection some ablation of the injector electrode and insulator occurred. Comparison of the ablated mass with the wall energy flux suggests that the energy flux needs to be reduced 10-20% per pulse to completely eliminate ablation caused by radiative melting of the surface.

The performance measurements can be improved with two changes in the system. First, a thruster which operates at 5-10 kW instead

of 500W would greatly improve the mass utilization. Second, improved pumping to drop the background pressure to the millitorr range would provide better performance as well as a capability for experimentally measuring the exhaust velocity.

This work has demonstrated technical feasibility for the water propellant PET thruster at 1000-2000 seconds. The efficiency is at least .50, and is conceivably as high as .75 at lower ambient pressure. Because liquid water injection is easier to accomplish at higher mass flow rates, the prime application of the PET thruster would seem to be for mean power levels of 5 kW and up. It should receive strong consideration for such missions.

V. ACKNOWLEDGEMENTS

We are grateful to Thom Chichester of GTD for many design and technical contributions, and to Steve Brown for the final design.

This work was supported in part by NASA-Lewis Research Center (Contract NAS3-24636) and in part by GT-Devices.

VI. REFERENCES

1. Burton, R. L., Goldstein, S. A., Hilko, B. K., Tidman, D. A., and Winsor, N. K., "Investigation of a Pulsed Electrothermal Thruster", Final Report No. NASA CR-168266, NASA-Lewis Research Center, October 1, 1983.

2. Burton, R. L., Goldstein, S. A., Hilko, B. K., Tidman, D. A., and Winsor, N. K., "Investigation of a Pulsed Electrothermal Thruster System", Final Report No. NASA CR-174768, NASA-Lewis Research Center, October 31, 1984.

3. Test of PET Thruster with water propellant. GT-Devices, Alexandria, VA, March 22, 1984.

4. Princeton University, Department of Electrical Engineering, Princeton, NJ.

5. Tidman, D. A. and Goldstein, S. A., "Thermal Transport to Hypervelocity Gun Tubes by High Pressure Partially Ionized Gas Flows," Tech Note GTD85-4, GT Devices, Alexandria, VA, May 1985.

6. Tidman, D. A., Thio, Y. C., Goldstein, S. A., and Spicer, D. S., "High Velocity Electrothermal Mass Launchers," Tech Note GTD 86-7, GT-Devices, Alexandria, VA, September 1986.

7. SESAME Equation of State Library, Report LASL-79-62, Los Alamos Scientific Laboratory, Los Alamos, NM.

8. Shapiro, A. H., "The Dynamics and Thermodynamics of Compressible Fluid Flow," Vol. I, The Ronald Press Company, New York, 1953, p. 101.

9. R. F. Hubbard, et.al, "Steady State Nozzle Flow Model for Sound Speed Dependent γ," Tech Note GTD85-1, GT-Devices, Alexandria, VA, January 1985.

APPENDIX A

VII. REPORT DISTRIBUTION LIST

	Copies
National Aeronautics and Space Administration Lewis Research Center 21000 Brookpark Road Cleveland, OH 44135	
ATTN: Willie C. Fleming, MS 500-312	1
Report Control Office, MS 60-1	1
Library, MS 60-3	2
Dr. M. Goldstein, Chief Scientist, MS 5-9	1
Lynnette M. Zana, MS 500-219	61
National Aeronautics and Space Administration Washington, DC 20546	
ATTN: RP/ Earl VanLandingham	1
RP/ Frank Stephenson, Jr.	1
RP/ Robert Wasel	1
Jet Propulsion Laboratory 4800 Oak Grove Drive Pasadena, CA 91102	
ATTN: J.F. Stocky	1
Dr. Graeme Aston	1
Technical Library	1
NASA Scientific and Technical Information Facility P.O.Box 8757 Baltimore, MD 21240	
ATTN: Accessioning Department	1
U.S. Air Force Rocket Propulsion Laboratory Edwards Air Force Base, CA 93523	
ATTN: LKC/Major Ed Huston	4
OSD/SDIO/IST Pentagon Washington, D.C. 20301-7100	
ATTN: Dr. Len Caveny	1

Aerospace Corporation
P.O. 92957
Los Angeles, CA 90009
ATTN: Dr. Ronald B. Cohen MS-754 1

Colorado State University
Fort Collins, CO 80521
ATTN: Dr. Paul J. Wilbur 1

Hughes Research Laboratories
3011 Malibu Canyon Road
Malibu, CA 90265
ATTN: DR. J.R. Beattie 1

RCA AstroElectronics
Box 800
Princeton, NJ 08540
ATTN: Dr. Kenn E. Clark 1

Rocket Research Corporation
11441 Willows Road
Redmond, WA 98052-9709
ATTN: William Smith, Engineering and Technology 1

TRW, Inc.
TRW Systems
One Space Park
Redondo Beach, CA 90278
ATTN: Robert Sackheim 1
Sid Zafran 1